oceannetworks.ca

OCEAN NETWORKS CANADA

Co-seismic Tsunami Hazard Assessment for Northwest Vancouver Island - Phase II

Sep 2023

AN INITIATIVE OF University of Victoria

Prepared by:

Reza Amouzgar
Soroush Kouhi

Ocean Networks Canada
2474 Arbutus Road,
Victoria, BC, Canada V8N 1V8
Email: info@oceannetworks.ca
Website: www.oceannetworks.ca

Report

This report was prepared by Ocean Networks Canada (ONC), as part of the Northwest Vancouver Island Tsunami Risk Assessment project, in collaboration with Northwest Hydraulic Consultants Ltd. (NHC), and in partnership with Strathcona Regional District (SRD). The objective of this report is to present the tsunami modelling methodology and results performed for the study area. For more details regarding the tsunami mapping and risk assessment, refer to the project's final report prepared by NHC.

Project Contact:

Soroush Kouhi, PhD
Applied Science Specialist, Project Manager
Ocean Networks Canada
Email: skouhi@uvic.ca

Contents

1. INTRODUCTION

Most large tsunamis are triggered by subduction earthquakes beneath the Pacific Ocean, mainly off southern Alaska and along the Cascadia Subduction Zone. Geological evidence of recent large tsunamis has been found in tidal marshes and coastal lakes on western Vancouver Island (Benson et al., 1997, Clague et al., 1994, 2000). The most vulnerable areas to future tsunamis of this type are the outer coasts and inlets of Vancouver Island, where damage to coastal communities would be large according to the outcome of computer tsunami models based on hypothetical bottom motions (Dunbar et al*.,* 1989, 1991). Several studies have investigated the tsunami hazard along the west coast of Canada from both distant sources (e.g., Alaska-Aleutian) (Rabinovich et al., 2019) and local sources (e.g., Cascadia Subduction Zones) (Hebenstreit et al., 1989, Murty et al. 1989). The focus of most of these studies has been on Victoria (Fine et al., 2018a, Associated Engineering, 2021), Boundary Bay (Fine et al., 2020, ONC, 2022), and southern parts of Vancouver Island, for instance, Port Alberni (Barua et al., 2007), while less work has been performed for the Northwest Vancouver Island.

The Strathcona Regional District (SRD) commissioned a tsunami risk study for the region in 2020 with funding from the Province of BC through the Union of BC Municipalities in collaboration with the Ka:'yu:'k't'h' / Che:k:tles7et'h' and the Nuchatlaht First Nation. The collaboration between Northwest Hydraulic Consultants Ltd. (NHC), Ocean networks Canada Society (ONC), and Northwest Seismic Consultants Ltd. (NSC) produced this comprehensive study. The purpose of this project was to better understand tsunami hazards and risk on the northwest coast of Vancouver Island by using tsunami modelling, community experience, and Indigenous Knowledge.

The study area for this assessment is broad, spans about 200 km from Nootka Sound northward to Cape Scott and includes the communities of Gold River, Tahsis, Zeballos, Port Alice, Winter Harbour, Quatsino, and Holberg, as well as several Indigenous nations including the Ka:'yu:'k't'h'/Che:k:tles7et'h' First Nations and Nuchatlaht First Nation, Ehattesaht/Chinehkint First Nations, Quatsino First Nations, Mowachaht/Muchalaht First Nations. Therefore, the project was split into two phases: Phase I of the project included Tahsis Inlet, Esperanza Inlet, and Kyuquot Sound, and was completed in 2022. The project resources and inundations maps for Phase I are published and now available online (www.srd.ca/tsunami-mapping). In Phase II, ONC partnered with NHC to expand the risk assessment to communities in Nootka Sound and Quatsino Sound, with the funding provided by The Lake Family's All One Fund. This report focuses on tsunami modeling of Phase II of the project.

In this report, detailed tsunami simulations were carried out to quantify the coastal tsunami hazard posed by local and distant sources using FUNWAVE-TVD model, a well-established tsunami prediction tool with demonstrated accuracy. In the following sections, the study area and tsunami sources are firstly described. The modelling details and tsunami scenarios will be discussed next, and finally, the model results will be presented.

2. STUDY AREA

Northwest Vancouver Island is renowned for its natural beauty and rich historical significance. Located along the western coast, this region faces potential tsunami hazards from both local sources like the Cascadia Subduction Zone and distant sources like the Aleutian Islands in Alaska. The area encompasses parts of the Strathcona Regional District (SRD) and Regional District of Mount Waddington (RDMW). Phase II of the project includes several communities, namely Gold River (waterfront), Port Alice, Winter Harbour, Quatsino, Holberg, as well as the Quatsino First Nation and Mowachaht/Muchalaht First Nation. Notable provincial parks in the region include Raft Cove and Cape Scott. Please refer to Figure 1 for the visual representation of the study area.

Figure 1: Northwest Vancouver Island study area. The blue shades on the map indicate the area covered in Phase I, while the dotted lines represent the extent of Phase II.

3. CO-SEISMIC TSUNAMI SOURCES

Multiple approaches can be employed to evaluate the tsunami hazard, such as the deterministic method (e.g., Wronna et al., 2015) and the probabilistic method (e.g., Geist and Parsons, 2006; Goda, 2022). For this particular project, we utilize a deterministic approach, wherein we identify and analyze the most substantial tsunami scenarios for the study area. The subsequent sections will elaborate on these selected scenarios.

3.1. Cascadia Subduction Zone

Great megathrust earthquakes occur in the Cascadia Subduction Zone roughly once every 500 years (Goldfinger et al., 2012). The last great Cascadia earthquake occured in 1700, and while there is no written record of the impact along the eastern Pacific, it was recorded in oral history (e.g., Ludwin et al., 2005) as well as in the coastal and offshore stratigraphy at sites from northern California to Vancouver Island (e.g., Atwater et al., 1995; Goldfinger et al., 2012).

For the Cascadia Subduction Zone tsunami source, the splay-fault rupture model developed by Gao et al. (2018) was selected from three types of rupture scenarios including buried rupture, splay-faulting, and trench-breaching. The low-resolution tsunami simulation indicated that the splay faulting rupture (Mw=9.0) can generate higher wave surface elevation compared to other rupture scenario (e.g., 50-100% higher compared to buried rupture scenario) (Gao et al., 2018). This suggests that splay-faulting scenario has the greatest potential impact on the BC west coast and SRD. The low-resolution tsunami simulation performed by ONC for the City of Prince Rupert also confirmed the higher surface elevation from a splay-fault rupture compared to other Cascadia fault ruptures (ONC, 2019). Figure 2 shows the initial vertical displacement of the Cascadia Subduction Zone rupture based on this scenario.

3.2. Alaska-Aleutian Subduction Zone

The Alaska-Aleutian Subduction Zone is the origin of numerous significant earthquakes of magnitude 8 and more (e.g., Mw 8.3 in 1938, 1946 Mw 8.6, 1957 Mw 8.6, 1964 Mw 9.2, 1965 Mw 8.7; see Dunbar and Weaver (2008) and Nelson et al. (2015)). The largest of the recent earthquakes, namely, the 1964 Alaska earthquake produced the largest instrumentally recorded tsunami waves to date on the British Columbia coast (Wigen and White, 1964), and this event represents a realistic proxy for similar large events generated by the subduction zone.

Numerical simulation of the 1964 tsunami in this study is based on the most recent co-seismic slip distribution for the Alaska 1964 rupture (Suleimani et al., 2020), constructed on the model of Suito and Freymueller (2009) (Figure 3). The authors applied the inversion-based model by Johnson et al. (1996) as a basis for their co-seismic slip model, adjusting it to an updated geometry. The revised model includes contributions from co-seismic horizontal displacements into the initial tsunami wave distribution through the component of the sea surface uplift due to horizontal movement of the steep sea floor slopes. Inclusion of deformation due to horizontal displacements can increase the far-field tsunami wave amplitudes in tsunami simulations.

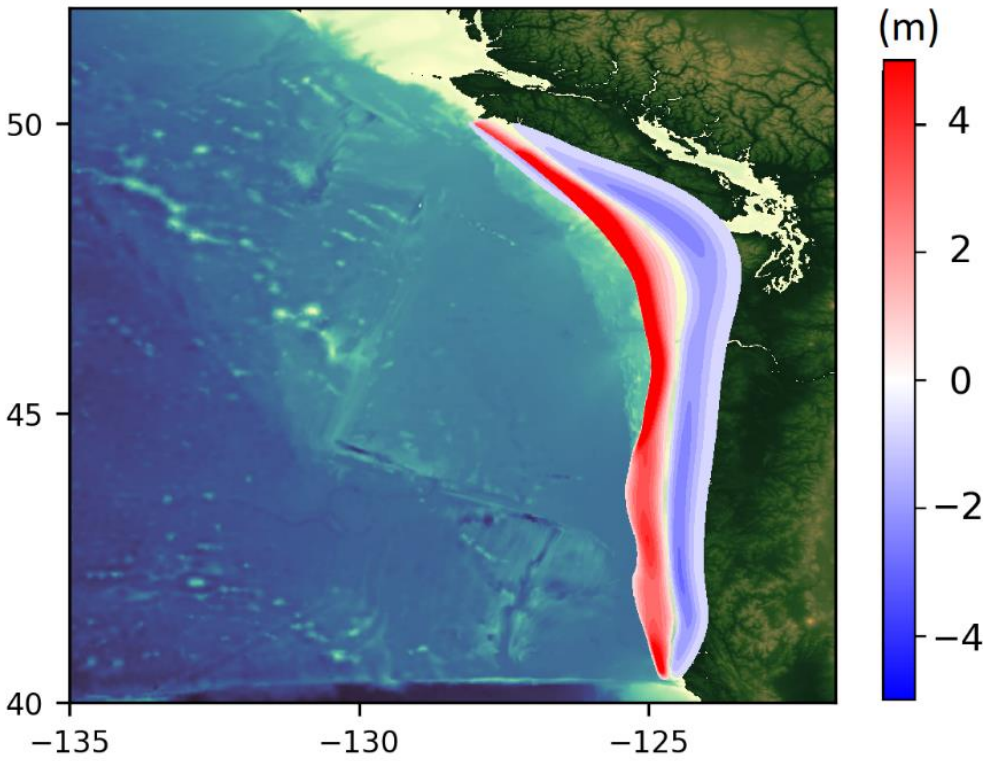

Figure 2: Seafloor vertical displacement (m) for the Cascadia Subduction Zone earthquake based on the splay faulting rupture model. Image was replotted from the provided data by Natural Resource Canada (NRCan) corresponding to Gao et al. (2018) where blue color shows the seafloor/topography subsidence and red color indicates seafloor uplift.

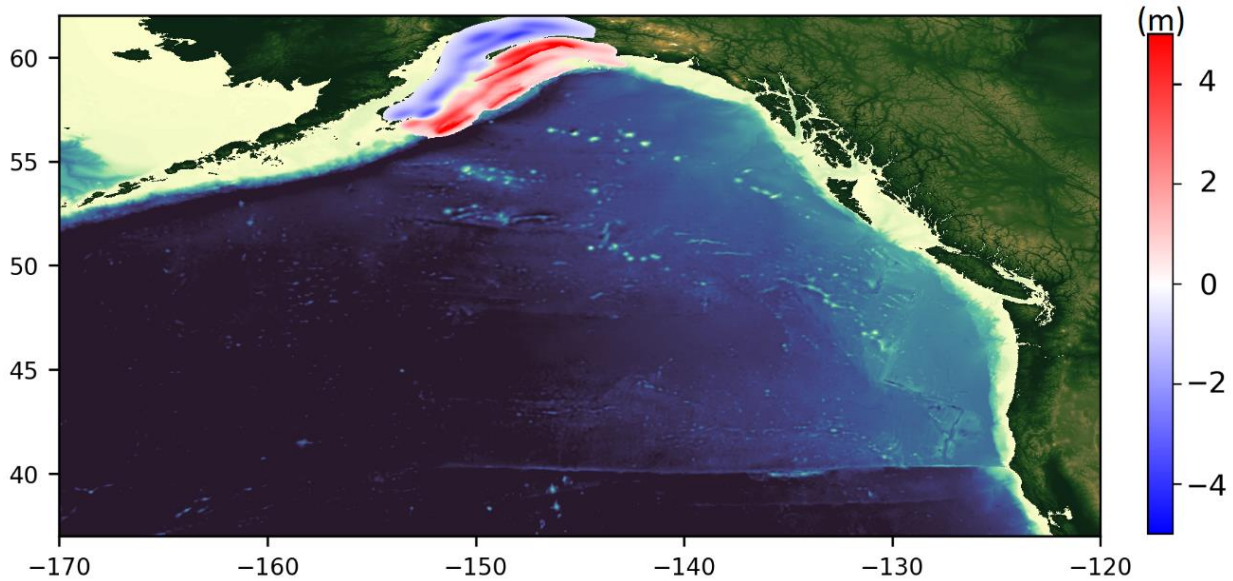

Figure 3: Seafloor vertical displacements (m) at the source region for the Alaska 1964 earthquake. Image was replotted from the provided data by University of Alaska Fairbanks corresponding to Suleimani et al. (2020) where blue color shows the seafloor/topography subsidence and red color indicates seafloor uplift.

4. HYDRODYNAMIC METHODOLOGY

Tsunami wave generation, propagation and inundation are commonly modelled using the 2D non-linear shallow water equations (SWE) and non-hydrostatic models. The non-linear shallow water equations can be derived in a number of methods, but all of them fundamentally arise from an integration of the Euler or Navier-Stokes equations with the assumption of vertically invariant horizontal velocity and hydrostatic pressure. These assumptions are usually correct for seismically generated tsunamis as the horizontal wavelength of tsunamis is much larger than the water depth scale. TUNAMI, COMCOT, and MOST are popular models based on the SWE which have been validated successfully through benchmarks using water level records from historical tsunami events (Imamura et al., 1988; Liu et al., 1994; Titov and Synolakis, 1998).

However, the SWE models lack the capability of simulating dispersive waves, which is the dominating features in landslide-generated tsunamis (Lynett and Liu, 2002) and is important for far-field tsunamis travelling a long distance (Grilli et al., 2012). Correspondingly, Boussinesq-type models represent an extension to SWE to better describe the wave dispersions, and multiple numerical models have been developed based on these equations, for instance, FUNWAVE-TVD a fully nonlinear Boussinesq wave model (Kirby et al., 1998 and Wei et al., 1995) or COULWAVE (Lynett and Liu, 2002). NEOWAVE (Non-hydrostatic Evolution of Ocean WAVEs) (Yamazaki et al., 2010) and NHWAVE (Non-Hydrostatic Wave Model) (Ma et al., 2012) are also 3D non-hydrostatic models that have been widely used for the generation and propagation of seismic and landslide-generated tsunamis.

Although nonlinear non-hydrostatic models can simulate complicated physics associated with wave dispersion, they are computationally more demanding. The numerical model FUNWAVE TVD used to examine the propagation of the tsunami waves is described in the following section.

4.1. Model description

The propagation and inundation of tsunamis induced by seismic events were modelled using the FUNWAVE-TVD model, a long wave propagation model that solves fully non-linear and dispersive Boussinesq wave propagation equations (Wei et al., 1995). This model employs a hybrid finite-volume and finite-difference scheme and has been developed both as a fully nonlinear version in cartesian coordinates (Shi et al., 2012) and a weakly nonlinear approximation in spherical coordinates (Kirby et al., 2013).

FUNWAVE-TVD has been benchmarked against other models and reference data in the U.S. as part of the National Tsunami Hazard Mitigation Program (NTHMP) (Horrillo et al., 2014), for hazard mapping along the U.S. coastline. The FUNWAVE-TVD model has been extensively used for tsunami modelling worldwide, for instance, modelling of a potential flank collapse of the Cumbre Vieja Volcano in the Atlantic Ocean, submarine mass failures along the US east coast (Grilli et al., 2015), interactions with tides (Shelby et al., 2016), tsunami hazard in the Mediterranean (Nemati et al., 2018), and recently co-seismic tsunami hazard assessment for Prince Rupert undertook by ONC in collaboration with NHC (ONC, 2019, 2022a, 2022b, 2023a).

4.2. Grid nesting

Accurate numerical simulation of tsunami waves in rapidly shoaling coastal regions requires setting up the model domain as a series of grids of finer spatial and temporal resolution. The use of nested grids makes it possible to resolve tsunami wave configurations as they propagate into increasingly shoaling coastal regions.

The use of nested grids for numerical modelling has several principal requirements: (1) grid cell sizes are obtained by dividing the initial, large-scale coarse numerical grid by an integer, typically 3 to 6. Integers larger than this can lead to grid interface problems. (2) nested grids are needed in near-coastal areas and the coarse "parent" grid should be of sufficient extent to resolve possible feedback effects that the nested grid may have on the parent grid during the simulation time. (3) high-resolution bathymetry, external forcing, and observations are needed for model domain setup, initialization, and validation at each domain level.

For this study, a series of nested grids (G1, G2, G3, G4, G5A, and G5D) was used to simulate the propagation of the potential tsunamis from the source regions to north coasts of Vancouver Island (Figure 4). It should be noted that grids G5B and G5C are specifically associated with Phase I of the project (ONC, 2022b). The resolution increases from the outer grid to the inner grid and is reported in Table 1. The wave elevations and horizontal water velocities are transferred from the coarser resolution to finer resolution grids at the boundaries.

The initial grid in spherical coordinates (G1) with a horizontal resolution of 2 arc-minutes is used for the initial source generation, which is necessary to reproduce tsunami waveforms in the Pacific with the FUNWAVE-TVD model (e.g., Kirby et al., 2013). To avoid non-physical reflections from boundaries of G1, an absorbing sponge layer of 200 km were applied to all boundaries. G1 is the coarsest numerical grid that covers the north pacific and includes the Alaska tsunami source region. As waves approach the area of interest, a second coarse resolution spherical mesh of 30 arc-seconds is used for the area covering most of the BC coastline encompassing the Cascadia Subduction Zone.

Table 1: Information of the numerical grids for the tsunami modelling.

Grid	Latitude	Longitude	Resolution
G1: Northeast Pacific	37° to 62°N	170° to 120°W	2 arc-min (~3000 m)
G2: Cascadia	40° to 52°N	135° to 121.76° W	30 arc-sec (~ 700 m)
G3: Vancouver Island	48.74° to 51.96° N	130.1° to 125.04° W	240 m
G4: Local region	49.05° to 51.39° N	129.41° to 125.74° W	60 m
G5A: Nootka Sound	49.26° to 49.93° N	126.86° to 125.84° W	10 m
G5D: Quatsino Sound	50.15° to 50.91° N	128.38° to 127.19° W	10 m

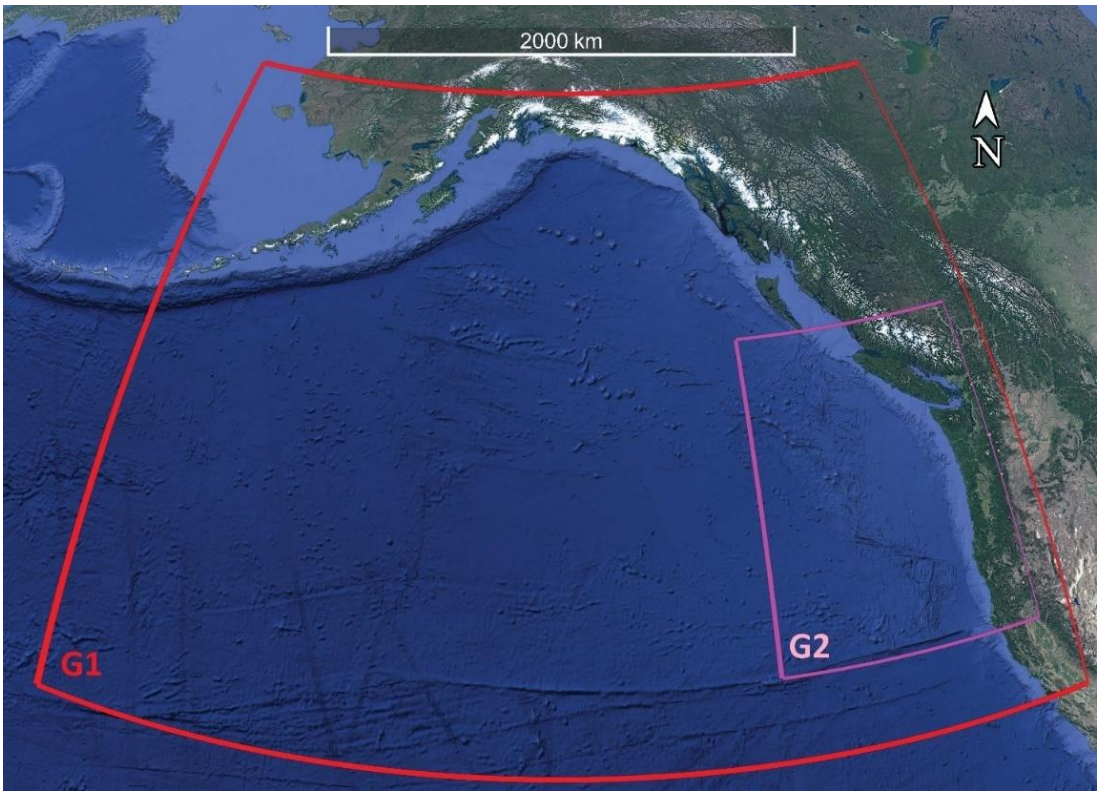

(a)

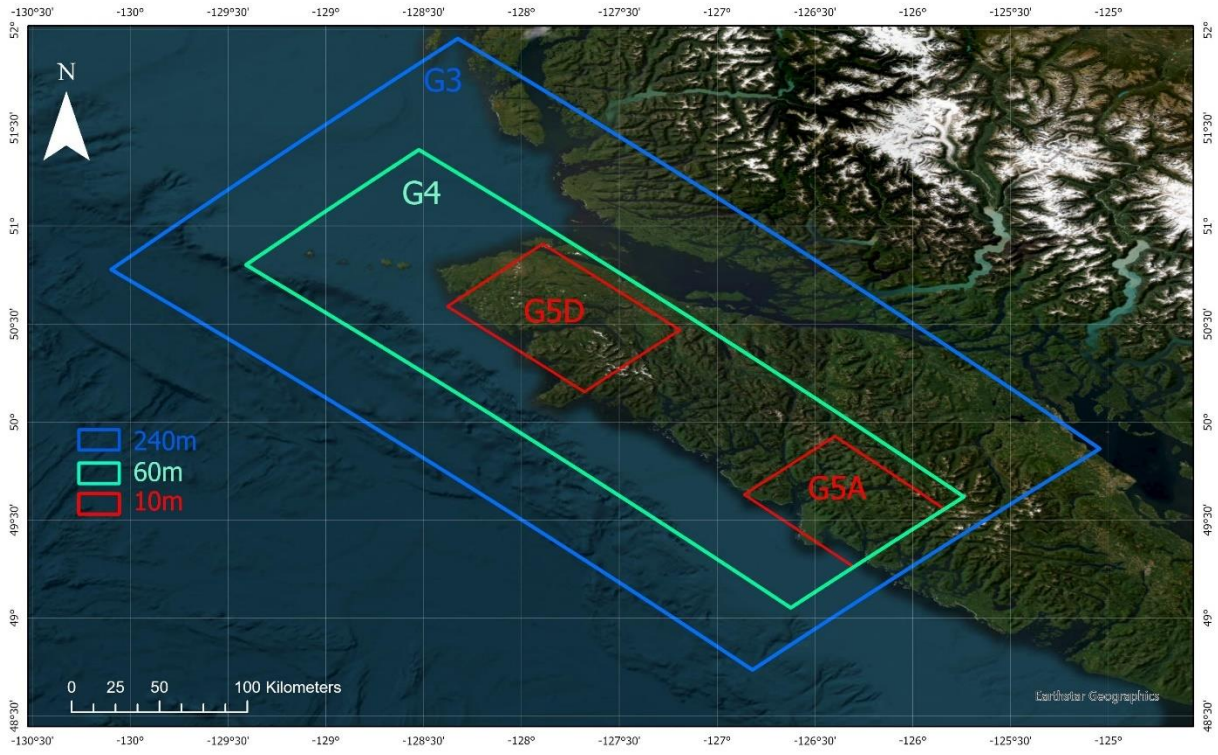

(b)

Figure 4: The arrangement of the nested grids: (a) spherical grids G1 and G2 with 2' and 30" resolutions, respectively; (b) cartesian grids G3, G4, G5A and G5D with 240 m, 60 m, 10 m, and 10 m, respectively. Note: grids G5B and G5C are specifically associated with Phase I of the project (ONC, 2022b).

In order to generate the Cartesian grids (Figure 4b), the spherical coordinates were projected on Cartesian coordinates using a Mercator projection. This projection is similar to UTM projection, with an origin located at 50° N and 127° W between the high-resolution grids (G5A and G5D), to minimize distortion to the grid as the wave propagates toward the shore. Moreover, in order to better align the higher resolution mesh with Vancouver Island coastlines and continental shelf, a 45° counter-clockwise rotation relative to the horizontal geographical coordinates at the region were applied to all cartesian grids. This rotation was also applied to the calculated output of the G2 results to accurately produce the boundary conditions at G3 boundary nodes.

G3 has an intermediate resolution of 240 m and can capture the energy exchange between the deep waters and shallower coastal zone. The nested grids are then refined to higher resolutions on the Cartesian grid, first to a 60m resolution grid (G4) and lastly to two 10 m resolution grids (G5A and G5D) covering the key study areas shown in Figure 1. G4 covers the waters surrounding Northwest Vancouver Island to account for wave transformation along the outer coast of the island. G5A and G5D have the highest spatial resolution of 10m, designed for the tsunami inundation modelling of the region.

The Manning coefficient n = 0.025 $s/m^{1/3}$ was assumed over the entire domain for all tsunami grids. This coefficient varies based on the roughness of the seabed, however, significant reduction in tsunami amplitudes may occur by using higher values of n in finer resolution grids (Schambach et al., 2018). Therefore, in the absence of land use data, they recommended using the conservative manning n coefficient n=0.025 for coarse sand.

4.3. Bathymetry and topography assimilation

Multiple bathymetric and topographic data were integrated to develop required high-resolution DEMs for the tsunami modeling. Topographic data was collected from the Light Detection And Ranging (LiDAR) survey for this study. Bathymetric data was mainly provided by the Canadian Hydrographic Service (CHS) in various resolutions. High-resolution multibeam existed for some inlets and coasts, however, to accurately model these areas, additional data was required for the high-resolution modelling which was acquired from surveying the areas that were not covered by the CHS data.

DEM development included data collection and review, DEM generation, and quality assurance and quality control (QAQC). Additional details of the topographic and bathymetric datasets used to develop the high-resolution DEM is reported in the DEM development appendix associated with this project, prepared by Ocean Networks Canada in collaboration with NHC (ONC, 2023).

4.4. Model vertical reference level

The US National Tsunami Hazard Mitigation Program (NTHMP, 2010) recommends to capture the contribution of high tide conditions, the inundation modelling takes place at a minimum of the US Mean High Water (MHW) level for a specific region. However, it is common to use US standard Mean Higher High Water (MHHW) as a more conservative tidal reference in such tsunami

modelling studies (Suleimani et al., 2013). The US standard Mean Higher High Water (MHHW) corresponds to Canadian standard Higher High Water Mean Tide (HHWMT), which has been used for various tsunami modelling projects in BC regions, for example, Victoria (AECOM, 2013), Seal Cove (Fine et al., 2018b), and Boundary Bay (Fine and Thompson, 2020). Accordingly, in this work, the tsunami modelling was performed with respect to the HHWMT, as the initial tide level.

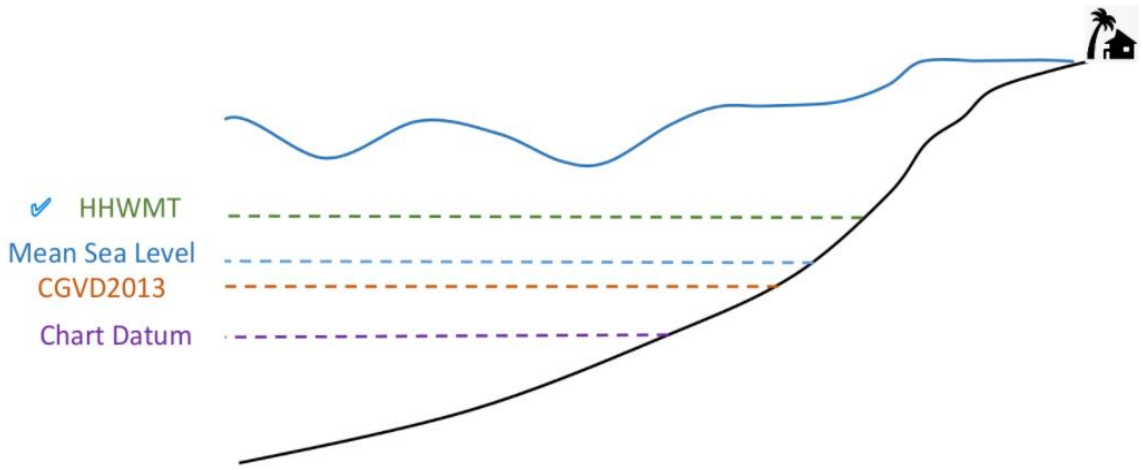

Figure 5: Schematic of vertical elevation references at the study area. HHWMT was used for tsunami modelling.

Figure 5 demonstrates the schematic of the vertical elevation references at the study area. The vertical reference of the DEMs developed for the tsunami modelling was relative to the Canadian Geodetic Vertical Datum (CGVD) 2013, which was translated to HHWMT for the modelling. To undertake this conversion, the HHWMT relative to Chart Datum (CD) were obtained for a number of key communities from the Canadian Tide and Current Tables (Fisheries and Oceans Canada, 2023).

CGVD2013 vertical reference levels with respect to CD along the BC coast were provided by CHS directly to ONC and is plotted in Figure 6. The conversion from CD to CGVD2013 were extracted from the CHS dataset and used to obtain values of HHWMT with respect to CGVD2013, as listed in Table 2 for the locations within the study area. Lastly, values of HHWMT with respect to CGVD2013 were averaged and presented in the last column of Table 2. For example, the Nootka Sound (G5A) which includes Saavedra Islands and Gold River, the HHWMT level on average is 1.5m above CGVD2013. Similarly, the HHWMT on average is 1.5m above CGVD2013 for Quatsino Sound (G5D) grid (see Table 2).

As a result, for modelling purposes at HHWMT, the DEM of these two grids (which were developed relative to CGVD2013) were uniformly lowered by 1.5m. Similarly, for 60m resolution grid, the averaged value of 1.5 m was applied for modelling. It should be noted for the first phase of the project, 1.5m was similarly calculated as the conversion value for modelling of G5B (Nuchatlitz) and G5C (Kyuquot) grids as well.

Table 2: Conversion of CGVD2013 to HHWMT by averaging the corresponding values for each grid of the study area. The listed CGVD2013 and HHWMT are relative to Chart Datum (CD).

Grid	Location	HHWMT (m, CD)	Elevation Datum Conversion (CD to CGVD2013)	HHWMT (m, GVD2013)	Averaged HHWMT for simulation (m, CGVD2013)
G5A	Saavedra Islands	3.6	-2.1	1.5	1.5
	Gold River	3.6	-2.1	1.5	
G5D	Hunt Islets	3.5	-2	1.5	1.5
	Port Alice	3.6	-2	1.6	
	Bergh Cove	3.5	-2	1.5	
	Kwokwesta Creek	3.6	-2.2	1.4	
	Makwazniht Island	3.4	-1.9	1.5	
	Coal Harbour	3.5	-1.9	1.6	

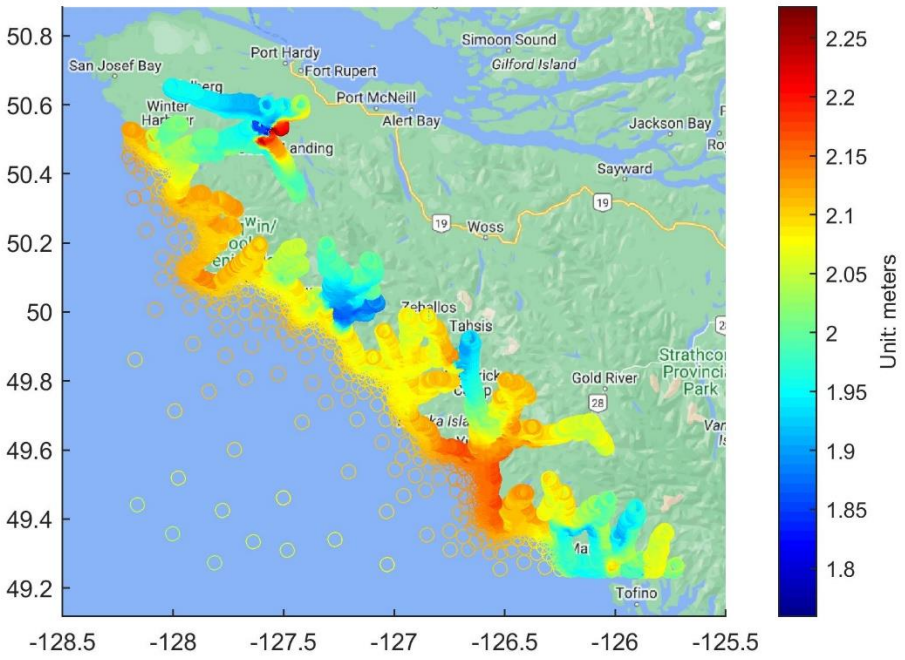

Figure 6: CGVD2013 spatial variation over the study area with respect to CD, provided by CHS directly to ONC.

4.5. Land subsidence/uplift

When considering tsunami impacts, land subsidence actively acts to increase the water elevation due to tsunamis and the subsided land will be more at risk to tsunami inundation. Subsidence within the study area is spatially variable, which is greater along the open coast and reduces further inland. It should be noted Nootka Sound would be relatively more affected by land subsidence due to its proximity to Cascadia subduction zone compared to Quatsino Sound. To account for the land deformation (subsidence/uplift) in the modelling process, the vertical deformation is simply superimposed to the underlying DEM.

4.6. Future sea level rise inclusion

Sea-level rise can noticeably increase the tsunami hazard, and even minor sea-level rise, can pose greater risks of tsunamis for coastal communities worldwide (Li et al., 2018). The sea level rise policy for the BC Ministry of Environment (Sandwell, 2011) recommends using 1.0 m rise in global mean sea level between the year 2000 and 2100 for planning purposes. In a recent study by NRCan (James et al., 2021), several average and enhanced SLR scenarios were studied for the water bodies surrounding Canada, which are based on different pathways of greenhouse concentration through the 21st century. For this project, the worst-case scenario of Projected Relative Sea-Level Change for Enhanced Scenario at 2100 was used for which additional meltwater from Antarctica is considered (Figure 7). This Enhanced SLR scenario predicts a maximum of 1.2 m of relative SLR along the coasts of Northwest Vancouver Island. For simulation of SLR scenarios in this project, the underlying DEM was lowered by 1.2 m for each tsunami scenario.

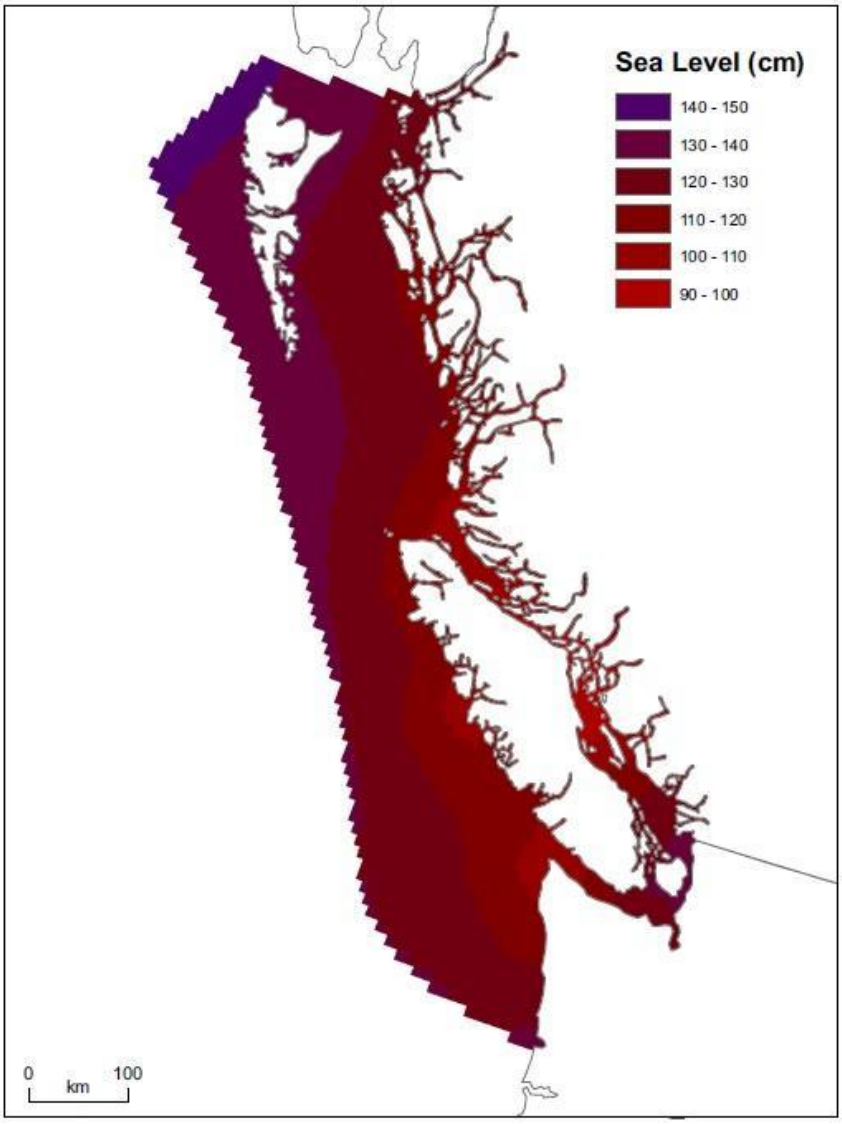

Figure 7: Projected Relative Sea-Level Change for Enhanced Scenario at 2100 along BC West Coast (James et al., 2021).

4.7. Modelling scenarios

A total of four tsunami scenarios were modelled which corresponding to present and future tsunami events. These scenarios include a local source event (Cascadia Subduction Zone) and distant source event (Alaska-Aleutian Subduction Zone) described in Sections 3.1 and 3.2, respectively under both present and future sea-level conditions:

- Scenario 1: Cascadia Subduction Zone, current-day sea-level conditions
- Scenario 2: Alaska-Aleutian Subduction Zone, current-day sea-level conditions
- Scenario 3: Cascadia Subduction Zone, future sea-level conditions
- Scenario 4: Alaska-Aleutian Subduction Zone, future sea-level conditions

The results of the 60m simulation were used to provide hazard information including wave amplitude, time of arrival, and tsunami-induced current velocities. The results of the high-resolution 10 m modelling were utilized for detailed inundation mapping for key study areas shown in Figure 1.

5. RESULTS

The following sections present the results of the tsunami simulation for three grids: the 60m grid, and the two high-resolution 10m grids, G5A (Nootka Sound) and G5D (Quatsino Sound). The outputs from the 60m simulation were used for overwater hazard mapping in the broader study area as well as the boundary conditions for the 10m modelling in Nootka Sound and Quatsino Sound. The results obtained from the 10m simulations was also utilized for inundation mapping. It is important to note that in this report, we provide the model outputs for the entire extent of each grid. For more detailed information on localized hazards and inundation mapping, please refer to the "Northwest Vancouver Island Tsunami Risk Assessment Final Report" prepared by NHC.

It is worth mentioning that in this study, the 240m and 60m resolution grids have been redesigned with larger extents compared to the grids used in the first phase of the project. This redesign was necessary to improve accuracy observed at the northern tip of Vancouver Island. The updated grid extents were expanded towards the north and west to overcome these issues.

To ensure the reliability and accuracy of the results, the consistency between the 240m and 60m resolutions at boundaries and offshore locations was first verified using the model results from the updated grid extents.

Additionally, as part of the quality assurance measures, the time series of water surface elevation obtained from the 60m and 10m model results were compared at various numerical gauge points. This comparison demonstrated a good agreement in the majority of the gauge points, further confirming the credibility of the model outputs.

The report utilizes various tsunami terminologies with the following definitions:

- Tsunami wave amplitude is defined as the vertical distance between the crest of a tsunami wave and a reference plane consisting of the still water level.

- The arrival time is defined the time of the first maximum of the tsunami waves (Intergovernmental Oceanographic Commission, 2019) following the trigger event. Flooding may begin before this moment is reached.

- Tsunami-induced currents are only generated by tsunami, and the tidal currents are not considered in modelling.

- Tsunami run-up is the highest vertical elevation upland reached by a tsunami with respect to a reference plane. This parameter is not directly reported in this document but can be obtained from the model results.

- For simplicity, Cascadia Subduction Zone and Alaska-Aleutian Subduction Zone tsunami sources are briefly referred as 'Cascadia' and 'Alaska', respectively.

- The simulation time for the Cascadia and Alaska scenarios were 6 and 9 hours, respectively. Tsunami wave parameters includes tsunami wave amplitude, tsunami wave arrival time, and tsunami-induced currents. In the case of the Cascadia scenario, which is in close proximity to the study areas, a test run revealed that a simulation time of 6 hours is adequate to capture the maximum wave parameters. On the other hand, for the Alaska scenario, it was determined that a minimum simulation time of 9 hours is necessary to account for the maximum tsunami wave parameters. It is important to note that longer simulation times could be employed for each scenario; however, this would increase computational costs without yielding significant additional benefits for the purpose of estimating the maximum tsunami wave parameters.

For better understanding of the tsunami impacts, the estimated amplitudes of the leading and maximum waves, as well as corresponding arrival times, were identified from the time series of water surface elevation at several numerical gauge points (GP). The location of the gauge points (GPs) is depicted in Figure 8 and listed in Table 3. The corresponding time series data obtained at these gauge points can be found in Annex A

It is important to mention that the numerical gauge points are situated a few meters away from the shoreline in deeper water. This placement allows for the representation of wave amplitudes over the water. However, it should be noted that when waves interact with the shoreline and propagate inland, they can cause water to surge to higher elevations, leading to the creation of an inundation zone. For detailed information regarding the levels of inundation for emergency planning, please refer to the main report of the project.

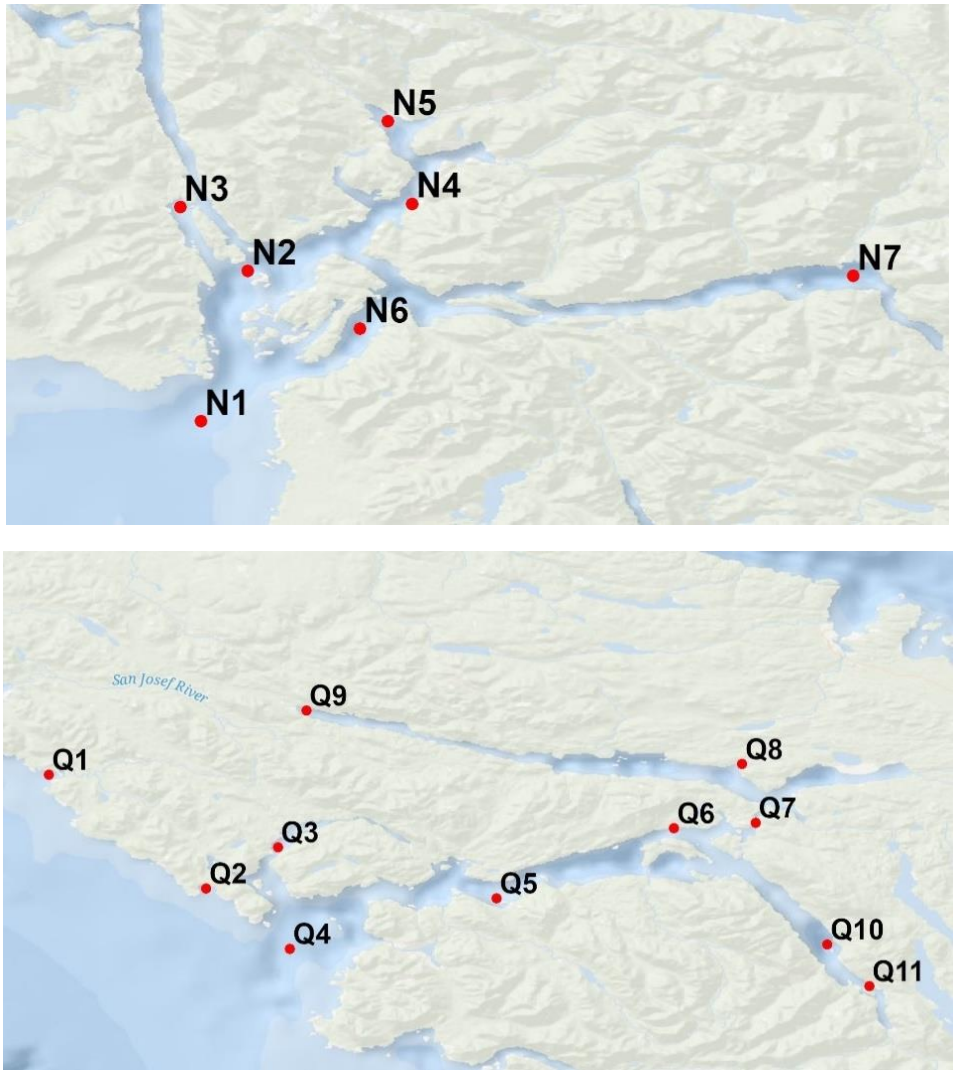

Figure 8: The location of several numerical gauge points (GPs) specified over the study area to obtain the time series of wave amplitude, top) Nootka Sound and bottom) Quatsino Sound See Table 3 for more details.

Table 3: The information of several numerical gauge points (GP) specified over the study area. See Figure 8 for the location of the GPs on the map.

GP	Location	Longitude	Latitude	GP No.	GP	Longitude	Latitude
N1	Nootka Sound entrance	-126.6231	49.5563	Q3	Winter Harbour	-128.0231	50.5158
N2	Eliza Passage	-126.5868	49.6724	Q4	Quatsino Sound entrance	-128.0115	50.4187
N3	Kendrick Inlet	-126.6391	49.7216	Q5	Mahatta River mouth	-127.8134	50.4669
N4	Cougar Creek mouth	-126.4594	49.7243	Q6	Quatsino	-127.6435	50.5339
N5	Head Bay	-126.4785	49.7881	Q7	Quatsino Narrows	-127.5653	50.5392
N6	Zucariate Channel	-126.4999	49.6277	Q8	Coal Harbour	-127.5781	50.5953
N7	Gold River waterfront	-126.1181	49.6685	Q9	Holberg	-127.9958	50.6466
Q1	Raft Cove	-128.2427	50.5853	Q10	Port Alice	-127.4965	50.4228
Q2	Grant Bay	-128.0921	50.4763	Q11	Port Alice terminal	-127.4564	50.3827

5.1. Cascadia Subduction Zone

5.1.1. Tsunami wave amplitude

The spatial distributions of maximum tsunami wave amplitudes from Cascadia event are illustrated in Figure 9. As a result of proximity to the Cascadia Subduction Zone, the tsunami amplitudes are generally higher toward the southern parts, in particular, from Brooks Peninsula toward south with the highest wave amplitude in Nootka Sound. In contrast, from Brooks Peninsula to Cape Scott in the northmost of Vancouver Island, including Quatsino Sound, the wave amplitudes reduce along the coast by distancing from the Cascadia subduction zone. More details about the maximum wave amplitude and arrival time of a Cascadia tsunami in Nootka Sound and Quatsino Sound are discussed in the next sections.

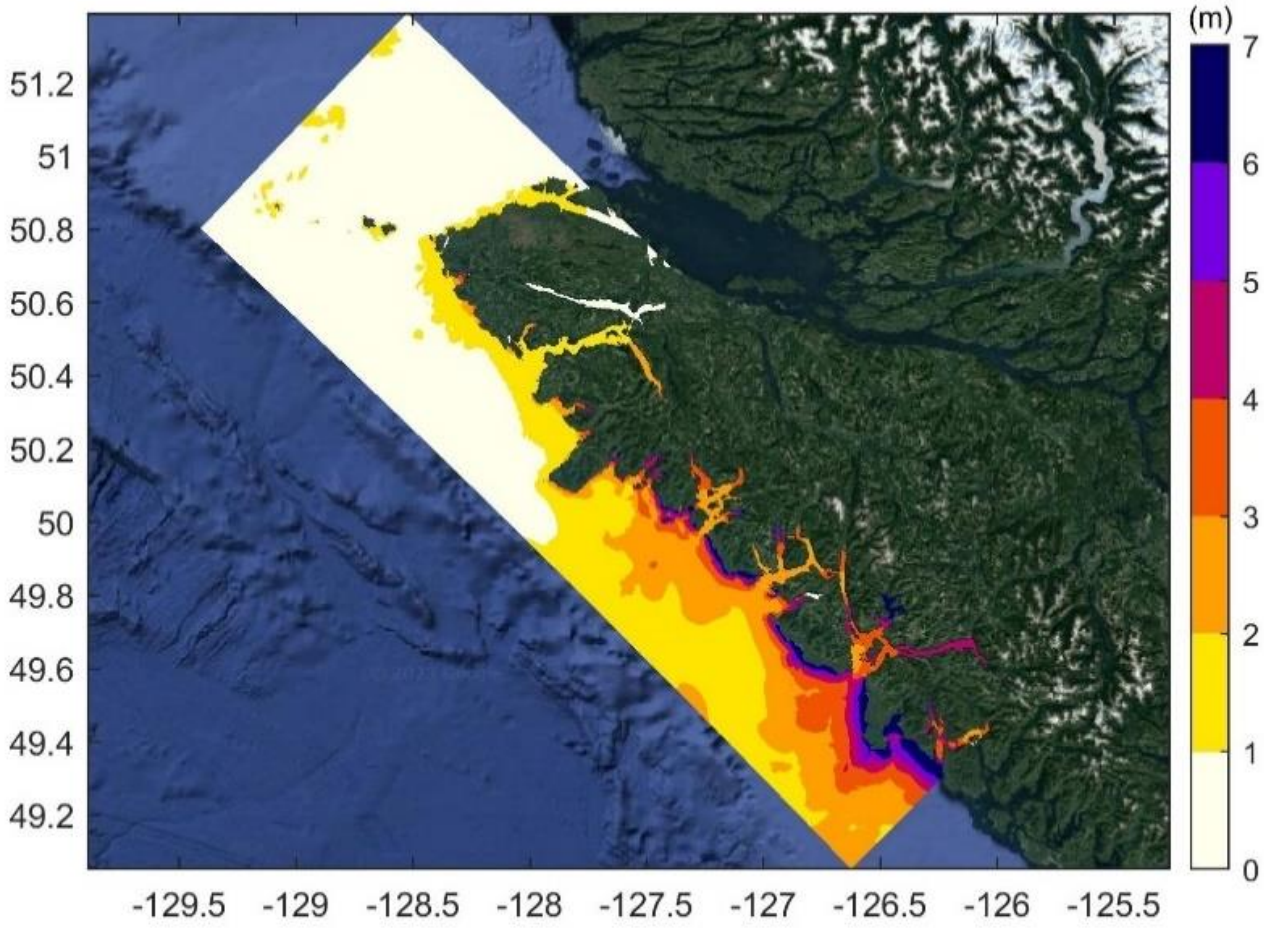

Figure 9: Maximum tsunami wave amplitude along Northwest Vancouver Island coasts for Scenario 1: Cascadia Subduction Zone current-day resulted from the 60 m resolution simulation.

Nootka Sound

Figure 10 shows the maximum wave amplitudes from the high-resolution simulation (10m) in Nootka Sound. The predicted amplitudes of the leading and maximum waves, as well as

corresponding arrival times were obtained from the time series of the water surface elevation (See Annexe A.1) at selected GPs (N1 – N7) and are listed in Table 4.

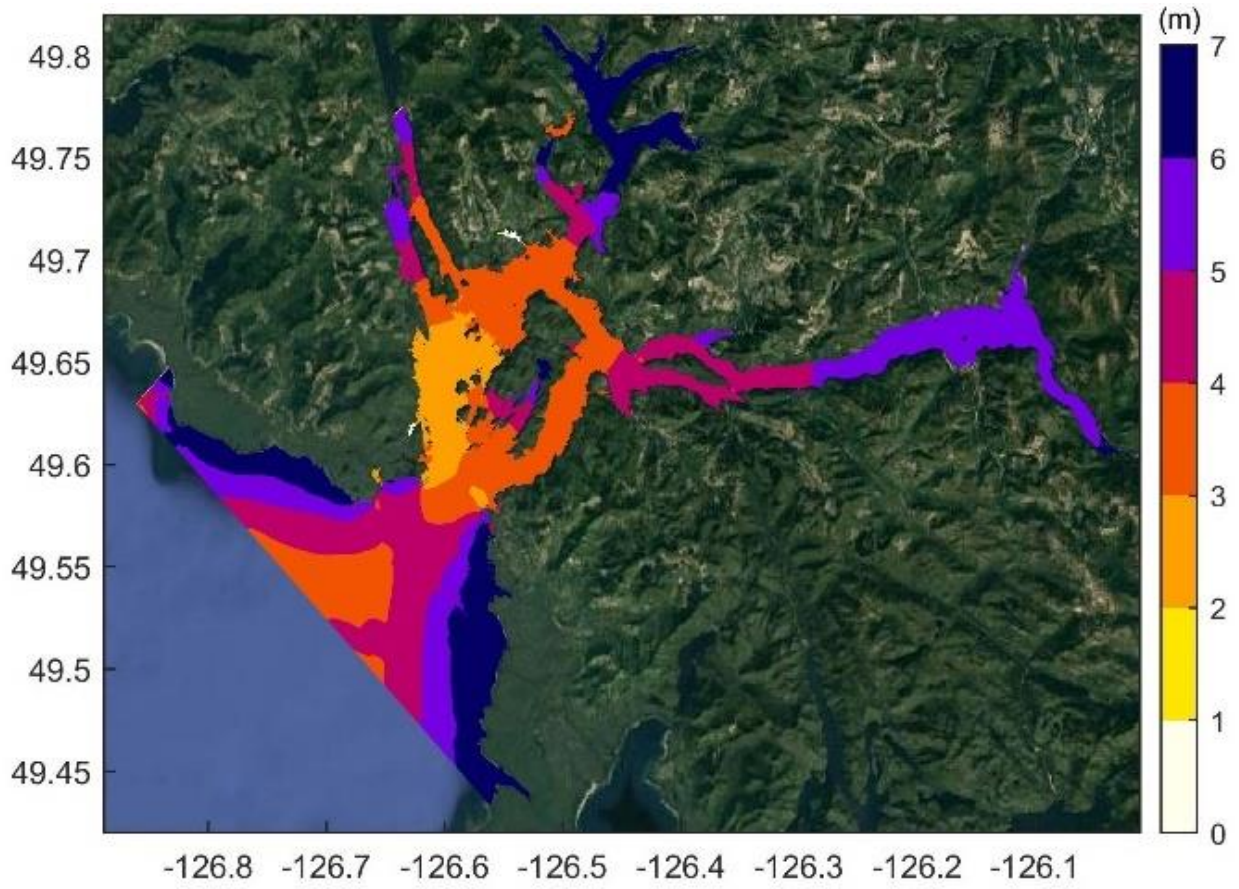

Figure 10: Maximum tsunami wave amplitude in Nootka Sound for Scenario 1: Cascadia Subduction Zone current-day resulted from the 10 m resolution simulation.

The wave amplitude at Nootka sound entrance (about 100 m depth) is about 4 m, where the funnel shape with shallower depths at the sides amplifies the wave to larger than 7 m. The wave would be dissipated as travelling into the sound (2 - 4 m), for instance to 2.9 m in Eliza passage (N2) before entering Tahsis inlet and 3.6 m in Zucariate Channel (N6) before entering the Muchalat Inlet. Inside Tahsis inlet and near to Strange Island the wave amplitude would be greater between 4-5m, for instance, it reaches 5.3 m at the end of Kendrick inlet (N3).

Similarly, at Gold River waterfront close to the end of Muchalat Inlet wave amplitudes of 5.5 m is predicted (N7). In this region, the model result from a 10m simulation predicts greater wave amplitude compared to 60m resolution (5.5m vs. 4.5m), as the higher resolution resolve the amplification more accurately, which may be the results of the resonance and reflection from the end of Muchalat Inlet. This pattern was also observed in the results of the Phase 1 of the project in this area.

As the tsunami waves propagating towards Tlupana Inlet, the tsunami wave is amplified to 5.6 at the mouth of Cougar Creek and when it reaches to Head Bay (N5), it exceeds 8m as the result of

the shoaling and potential resonance. It is also estimated that the tsunami wave amplifies at the end of Hisnit Inlet up to about 7m and spill over into Deserted Lake.

For the Cascadia tsunami in the Nootka Sound, the time series show that the first tsunami wave (peak) has the largest wave amplitude as a result of proximity to the subduction zone. The arrival time of the first maximum wave is estimated less than an hour from the earthquake occurrence, except at the Gold River waterfront which experiences the first maximum wave amplitude after about 1hr:15min.

Table 4: Tsunami maximum wave amplitudes and arrival times of Nootka Sound for Cascadia Subduction Zone current-day scenario at selected numerical gauge points (GP) displayed in Figure 8.

		First wave		Maximum wave	
GP	Location	Arrival time HH:MM	Amplitude (m)	Arrival time HH:MM	Amplitude (m)
N1	Nootka Sound entrance	00:28	4.2	00:28	4.2
N2	Eliza Passage	00:43	2.9	00:43	2.9
N3	Kendrick Inlet	00:45	5.3	00:45	5.3
N4	Cougar Creek mouth	00:47	4.5	00:51	5.6
N5	Head Bay	00:50	8.2	00:50	8.2
N6	Zucariate Channel	00:36	2.6	01:06	3.6
N7	Gold River waterfront	00:59	4.3	01:15	5.5

Quatsino Sound

Figure 11 shows the maximum wave amplitudes resulted from the high-resolution simulation (10m) in Quatsino Sound for a Cascadia tsunami. The predicted amplitudes of the leading and maximum waves, as well as corresponding arrival times at selected GPs (Q1 – Q11) are listed in Table 5. This information was obtained from the time series of the water surface elevation (See Annexe A.2).

The tsunami wave amplitude is between 2-3 m along the coasts of the Northwest of Vancouver Island. Offshore of the Raft Cove (Q1) and Grant Bay (Q2), the wave amplitude can reach to 3m.

The wave amplitude is estimated between 1-2m entering the Quatsino Sound (about 1.4 m at Q4). The maximum wave amplitude at Winter Harbour area predicted up to 3 m, although at the selected GP, it is about 1.9m (Q3). The wave has an of amplitude of 1.4 m at the mouth of Mahatta River (Q5) which increases to 1.7m at Hamlet of Quatsino (Q6), while at Hecate Cove the wave estimated to increase further to about 2.7m due to the shape of the cove.

The tsunami wave reaches up to 2 m at Quatsino Narrows (Q7), but dissipated as the wave passes through this narrow and shallow passage (reaches to about 200 m in width and as low as 30m in depth) to wider and deeper area (about 100m depth) towards Rupert and Holberg Inlets. Maximum wave amplitude would be smaller than 0.5m in these inlets (e.g., 0.4 m at Coal Harbour (Q8)), although at the end of Holberg inlet (Q9) the wave amplitude increases up to about 1 m.

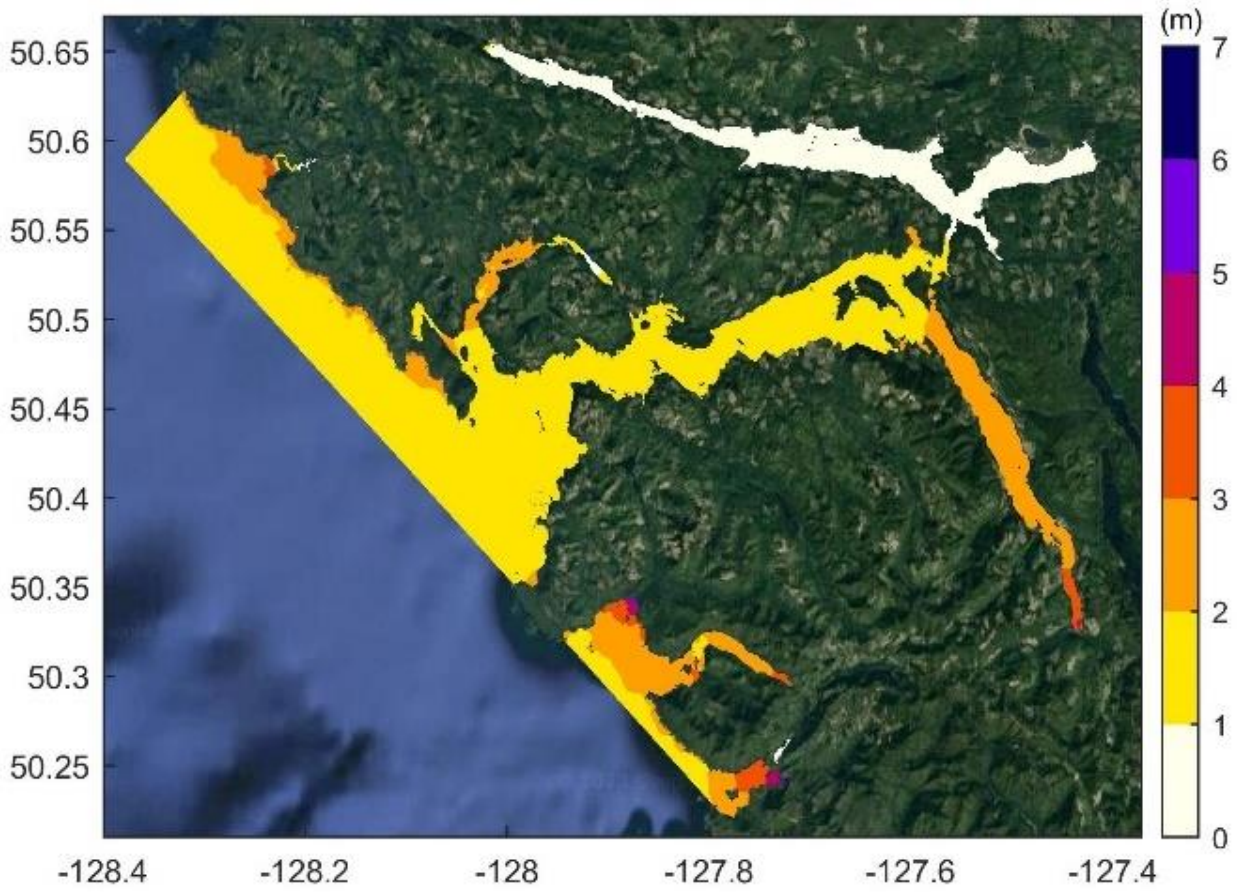

Figure 11: Maximum tsunami wave amplitude in Quatsino Sound for Scenario 1: Cascadia Subduction Zone current-day resulted from the 10 m resolution simulation.

In contrast, the wave which travels from Drake Island towards Port Alice through Bochholz Channel and Neroutsos Inlet is estimated 2.6 m at Port Alice (Q10) and its terminal (Q11). The wave would be amplified up to 4 m at the end of the Neroutsos Inlet due to shoaling in the shallower depths.

The first tsunami wave arrives to Quatsino Sound entrance in about 18 minutes. The arrival time of the first maximum wave for most gauges occur in less than an hour from the earthquake. However, the areas located in Holberg Inlet, Rupert Inlet, experience the first tsunami wave after about 1hr:30min from the earthquake (see Q8 and Q9). In Port Alice, the first maximum wave amplitude arrives about 1 hour from the earthquake (Q10 and Q11).

The time series also show that in most gauges the first tsunami wave (peak) is not the largest wave amplitude. For example, the first tsunami wave with 1m amplitude arrives to Port Alice after about 1 hour, whereas the largest wave with 2.6 m amplitude arrives about 3 hours from the earthquake (see Q10). It should be noted, however, for Nootka grid (presented in previous section), the first tsunami wave was the largest compared to the trailing waves at most gauges, as a result of proximity to the Cascadia tsunami source. According to the time series, the largest peak occurs within 1.5 hour inside Nootka Sound while within 5 hours in Quatsino Sound.

Table 5: Tsunami maximum wave amplitudes and arrival times of Quatsino Sound for Cascadia Subduction Zone current-day scenario at selected numerical gauge points (GP) displayed in Figure 8.

GP	Location	First wave		Maximum wave	
		Arrival time HH:MM	Amplitude (m)	Arrival HH:MM	Amplitude (m)
Q1	Raft Cove	00:26	2.2	02:18	2.9
Q2	Grant Bay	00:22	2.1	03:25	2.8
Q3	Winter Harbour	00:35	1.1	03:34	1.9
Q4	Quatsino Sound entrance	00:18	0.7	03:29	1.4
Q5	Mahatta River mouth	00:30	0.7	02:45	1.4
Q6	Quatsino	00:38	0.5	02:54	1.7
Q7	Quatsino Narrows	00:45	0.8	04:51	1.4
Q8	Coal Harbour	01:22	0.3	01:40	0.4
Q9	Holberg	01:35	0.5	03:28	0.8
Q10	Port Alice	00:57	1.4	03:02	2.7
Q11	Port Alice terminal	01:00	2.1	03:05	2.6

5.1.2. Tsunami-induced current velocities

The maximum tsunami-induced currents for Cascadia event is shown in Figure 12. As a result of proximity to the Cascadia Subduction Zone, the tsunami-induced currents are generally higher toward the southern parts of the broader study area, in particular, from Brooks Peninsula toward south, including Nootka Sound. In contrast, from Brooks Peninsula to Cape Scott in the northmost of Vancouver Island, including Quatsino Sound, tsunami-induced currents reduce along the coast by distancing from Cascadia tsunami source. On average, tsunami-induced currents offshore of Nootka Sound entrance is up to 2m/s while offshore of Quatsino Sound is lower than 1m/s. Quantitative tsunami-induced currents of Nootka Sound and Quatsino Sound from Cascadia event are discussed below.

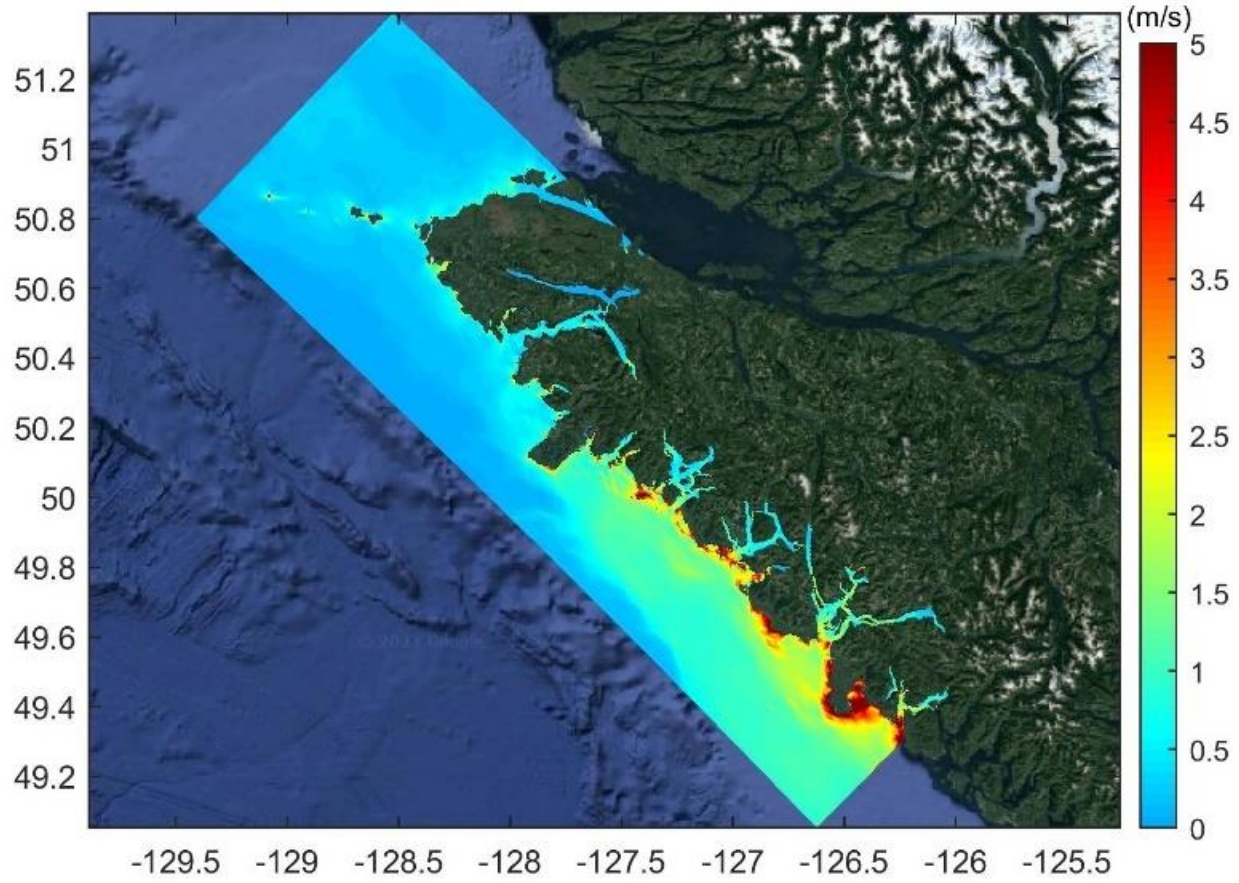

Figure 12: Maximum tsunami current velocities along Northwest Vancouver Island coasts for Scenario 1: Cascadia Subduction Zone current-day resulted from the 10 m resolution simulation.

Nootka Sound

The maximum tsunami-induced currents of the Cascadia tsunami simulation for Nootka Sound grid are shown in Figure 13. At entrance of Nootka Sound in deeper water, the tsunami currents of between 1.5 - 3 m/s estimated. However, at the sides of Nootka entrance due to its funnel shape and shallow depth the strong currents may exceed 5 m/s which, consistent with higher wave amplitude at these locations.

Within Nootka Sound tsunami-induced currents predicted in the range of 1-2 m/s at many regions. The tsunami currents, however, are stronger close to small island and narrow waterways. For example, in Hanna Channel close to Beligh Island tsunami-induced current of up to 5m/s are predicted. Similarly, at King and Williamson Passages in Muchalat Inlet in the vicinity of Gore Island where the tsunami wave propagates towards Gold River the tsunami-induced current larger than 5m/s are estimated.

In deep area of Gold River Terminal (i.e., greater than 100m), tsunami-induced currents less than 1m/s are predicted, however in shallower area and close to Gold River Highway larger tsunami currents about 2m/s are expected. In contrast, in Head Bay and Nesook Bay strong tsunami currents larger than 5m/s is estimated as the result of the shallower depth and wave runup over land. Please refer to the tsunami-induced current maps for additional details at specific areas of interest.

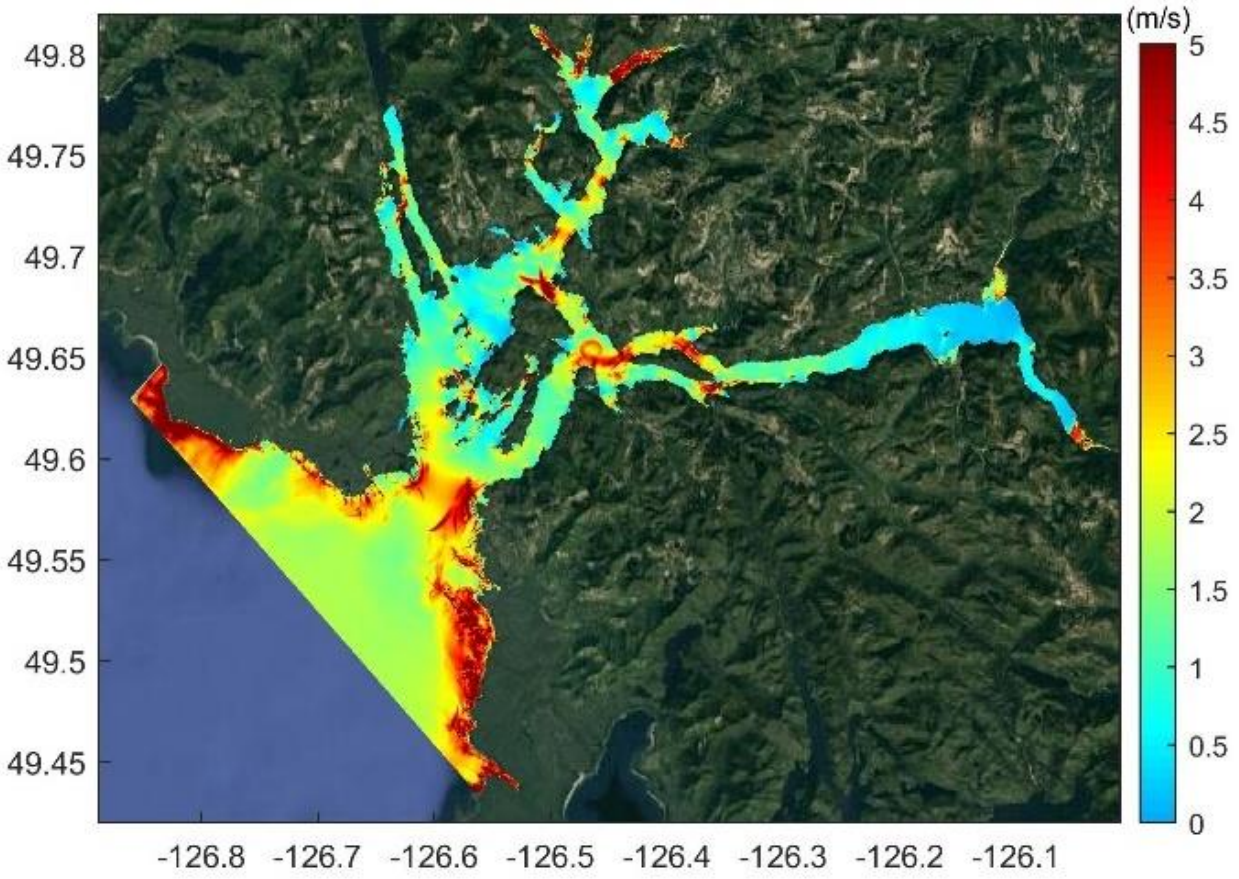

Figure 13: Maximum tsunami current velocities in Nootka Sound for Scenario 1: Cascadia Subduction Zone current-day resulted from the 10 m resolution simulation.

Quatsino Sound

The maximum tsunami-induced currents of the Cascadia tsunami in the Quatsino Sound is shown in Figure 14. In general, tsunami-induced currents in Quatsino Sound would be slower than Nootka Sound, as the result of the proximity with the Cascadia subduction zone and greater tsunami amplitude in Nootka Sound.

At northwest coast of Vancouver Island from Grant Bay toward north, the tsunami currents between 1.5 - 5 m/s is estimated, where recreational areas such as at Raft Cove are located. At entrance and inside the Quatsino Sound the tsunami currents of up to 1 m/s estimated. However, in narrow waterways, channels and close to small islands stronger tsunami currents are expected. For example, close to Quattische Island and Quatsino narrows tsunami currents larger than 3 m/s are estimated. Similarly, in Forward Inlet at Winter Harbour where the geometry is constricted and the depth is relatively shallow (e.g., about 20 m) strong currents larger than 5 m/s are simulated.

In Holberg Inlet, tsunami currents are small; for instance, in Coal harbour tsunami-induced currents are very small (less than 0.5 m/s), however, at the end of the inlet at Holberg it can exceed 1m/s. In Neroutsos Inlet where the tsunami wave propagates towards Port Alice,

tsunami-induced currents are up to about 0.5m/s, while in Port Alice terminal which has shallower depth the currents may exceed 3 m/s.

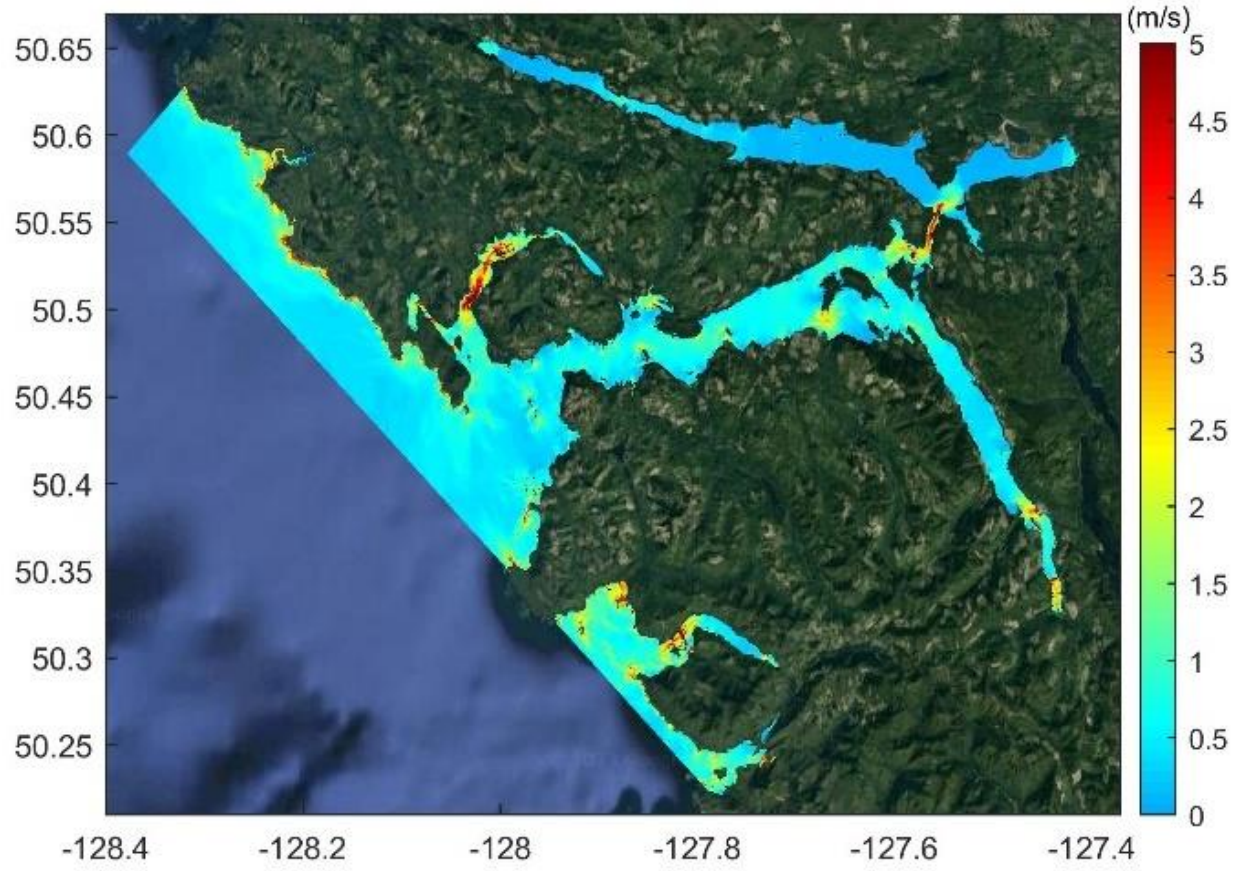

Figure 14: Maximum tsunami current velocities in Quatsino Sound for Scenario 1: Cascadia Subduction Zone current-day resulted from the 10 m resolution simulation.

5.2. Alaska-Aleutian Subduction Zone

5.2.1. Tsunami wave amplitude

The maximum tsunami wave amplitudes from Alaska event are illustrated in Figure 15. Unlike the Cascadia scenario, the maximum tsunami amplitudes are almost uniform in the range of 1 to 2 m along the western coast of Vancouver Island. This is due the tsunami propagation from a distant source, maintaining the physical characteristics of the waves almost unchanged along Vancouver Island coasts. More details regarding the maximum tsunami wave amplitude and arrival time of Nootka Sound and Quatsino Sound from Alaska event are discussed below.

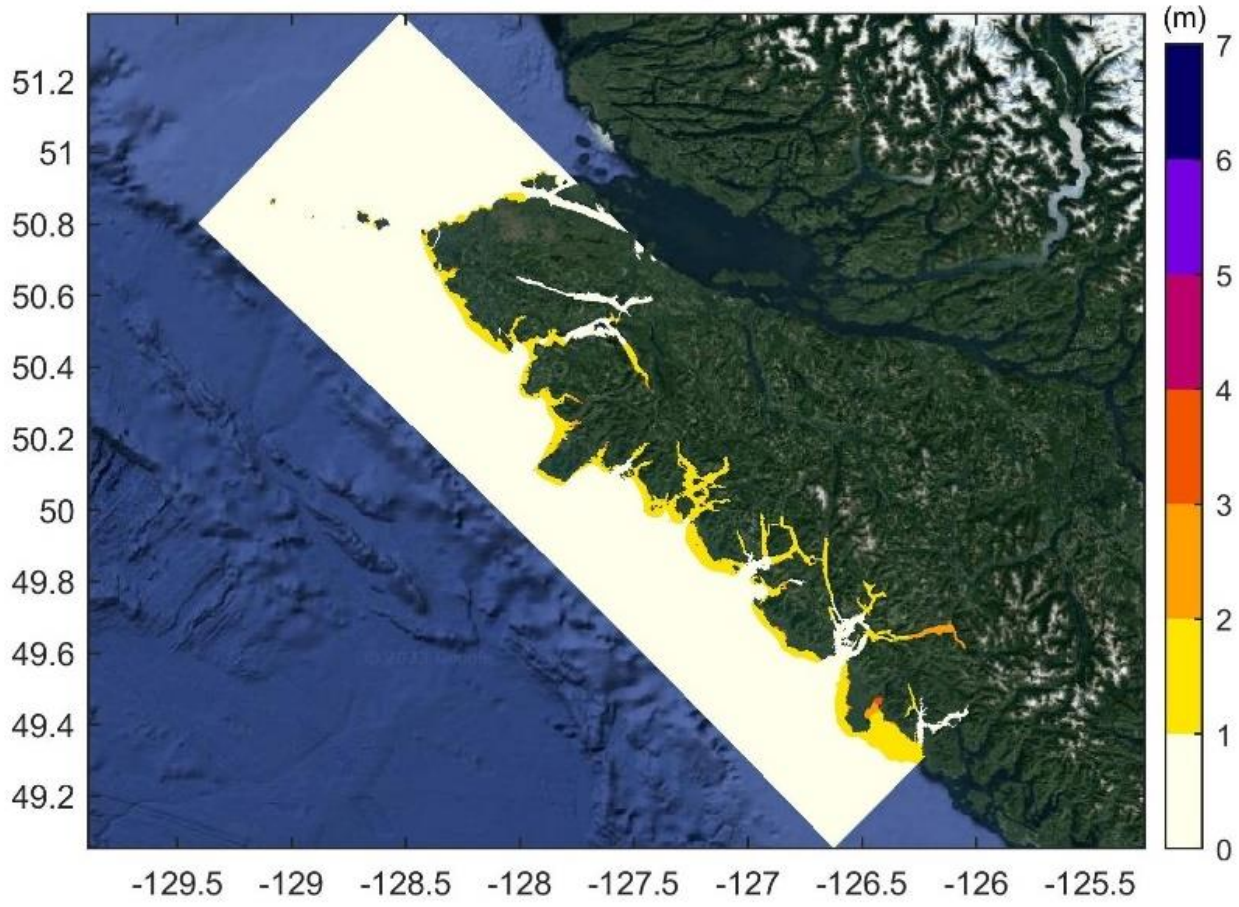

Figure 15: Maximum tsunami wave amplitude along Northwest Vancouver Island coasts for Scenario2: Alaska-Aleutian current-day resulted from the 60 m resolution simulation.

Nootka Sound

Figure 16 shows the maximum wave amplitudes resulted from the high-resolution simulation (10m) in Nootka Sound for an Alaska tsunami. The predicted amplitudes of the leading and maximum waves, as well as corresponding arrival times at selected GPs (N1 – N7) are listed in Table 6. This information was obtained from the time series of the water surface elevation (See Annexe A.3)

The wave amplitude at Nootka sound entrance (N1) is estimated up to 1m at the inner parts of the passage and up to 2 m at the sides of the passage. The wave amplitude will remain up to 1m at Yuquot, McKay Passage, Cheesish, and Critter Cove as well as at Eliza Passage (N2). While it amplifies to 1.2 m at Kendrick Camp (N3) and Cougar Creek (N4).

As the tsunami waves propagate towards the end of the inlets, the tsunami waves are amplified due to shoaling and potential resonance. At Head Bay (N5), the maximum wave amplitude of about 1.6m and at Gold River waterfront (N7), an amplitude of 3.2m is predicted. Similar to Cascadia tsunami in Muchalat Inlet, 10m resolution model results predict larger wave amplitude compared to 60m resolution model results.

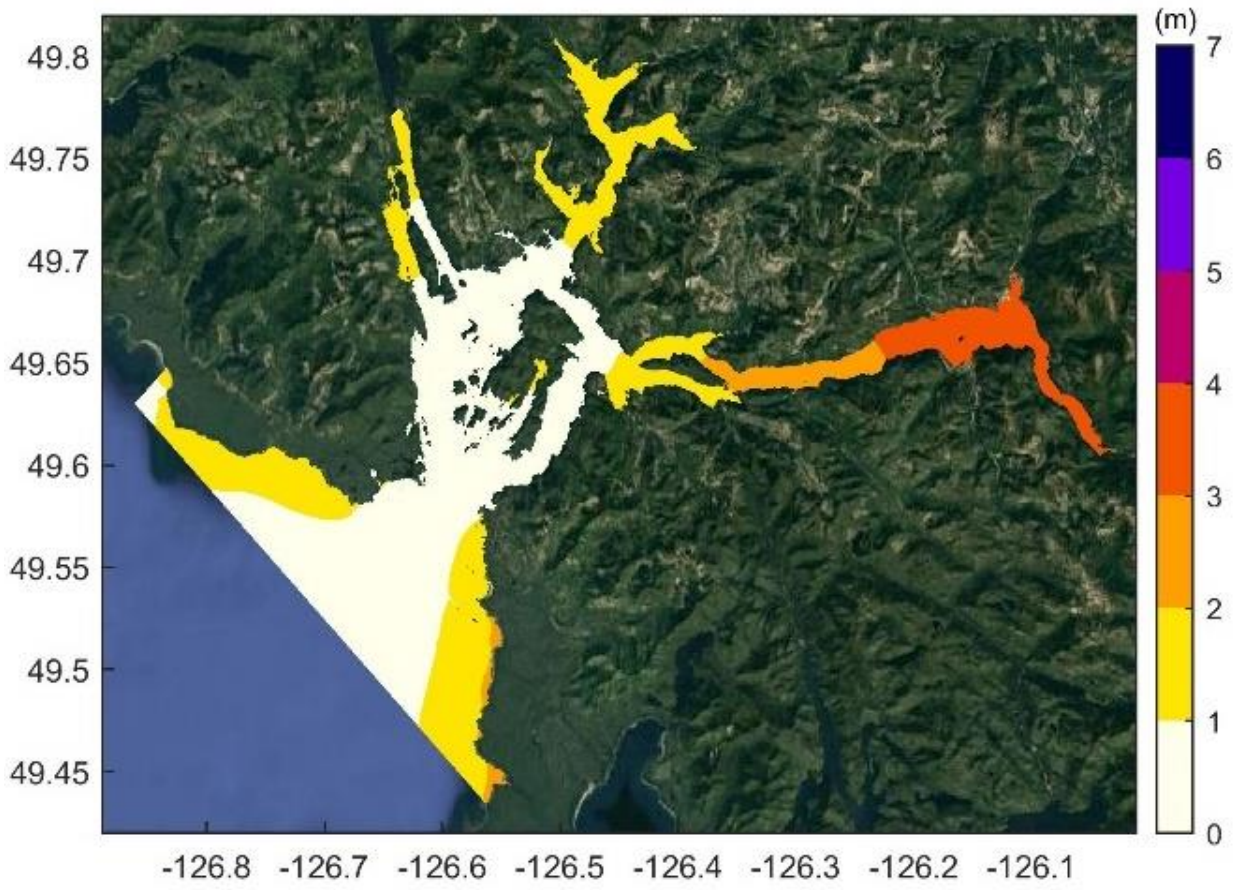

Figure 16: Maximum tsunami wave amplitude in Nootka Sound for Scenario2: Alaska-Aleutian current-day resulted from the 10m resolution simulation.

It is expected the first tsunami wave to arrive to all GPs after about 3 hours. The trailing waves may be larger compared to the first tsunami wave. For example, Gold River waterfront (N7) experiences a maximum wave amplitude of 3.2 m after about 7hr:12min.

Table 6: Tsunami maximum wave amplitudes and arrival times of Nootka Sound for Alaska-Aleutian current-day scenario at selected numerical gauge points (GP) displayed in Figure 8.

		First wave		Maximum wave	
GP	Location	Arrival time HH:MM	Amplitude (m)	Arrival time HH:MM	Amplitude (m)
N1	Nootka Sound entrance	03:13	0.8	07:38	0.9
N2	Eliza Passage	03:27	0.7	06:52	0.9
N3	Kendrick Inlet	03:29	1	06:55	1.2
N4	Cougar Creek mouth	03:32	0.9	05:33	1.2
N5	Head Bay	03:36	1.5	05:35	1.6
N6	Zucariate Channel	03:21	0.6	06:56	0.8
N7	Gold River waterfront	03:44	1.1	07:12	3.2

Quatsino Sound

Figure 17 shows the maximum wave amplitudes resulted from the high-resolution simulation (10m) in Quatsino Sound for an Alaska tsunami. The predicted amplitudes of the leading and maximum waves, as well as corresponding arrival times at selected GPs (Q1 – Q11) are listed in Table 6. This information was obtained from the time series of the water surface elevation (See Annexe A.4).

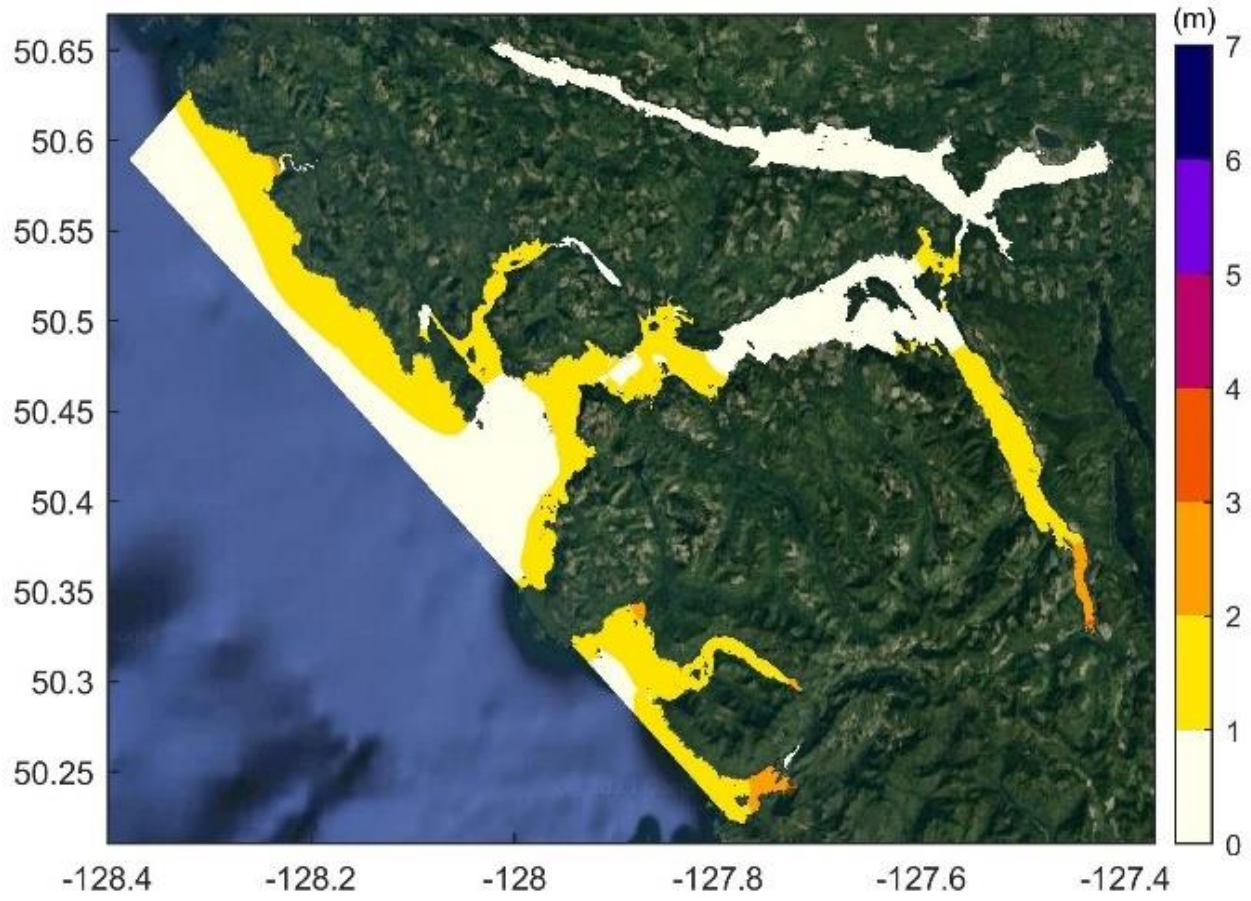

Figure 17: Maximum tsunami wave amplitude in Quatsino Sound for Scenario2: Alaska-Aleutian current-day resulted from the 10m resolution simulation.

Near to the coastlines of Northwest Vancouver Island the wave amplitude estimated to be between 1-2 m, for example, offshore of Raft Cove (Q1) and Grant Bay (Q2), the wave amplitude is estimated 1.8 m.

At the entrance the Quatsino Sound, wave amplitude is estimated up to about 1m for the Alaska tsunami (e.g., 0.8 m at Q4). The tsunami wave amplitudes are relatively consistent between 0-1 m at both 'Nootka Sound' and 'Quatsino Sound' entrances due to distance from the seismic source. Moving inside the sound, at Winter Harbour where the geometry is constricted and the depth is relatively shallow (e.g., about 20m) the wave amplitude of up to 2 m is estimated (e.g., 1.2 m at Q3). The wave amplitude at the Hamlet of Quatsino is about 0.9 m (Q6).
Within Holberg Inlet, the wave amplitudes are attenuated after passing through Quatsino Narrows. The wave amplitude at Coal Harbour (Q8) would be about 0.4m. At Holberg (Q9), the

10m resolution grid predicts larger wave amplitude (0.8 m) compared to 60m resolution grid, as the Quatsino Narrows is resolved more accurately with the higher resolution grid (10m).

The wave which travels from Drake Island towards Port Alice through Bochholz Channel and Neroutsos Inlet would be amplified due to shoaling in the shallower depths at the end of the Inlet. The maximum wave amplitude at Port Alice (Q10) and its Terminal (Q11) is estimated about 1.3 m and 1.8 m, respectively.

The first tsunami wave will arrive the entrance of Quatsino Sound after about 2hr:50min from the earthquake (Q4). While the first tsunami wave predicted to reach other gauges between 3-4 hours from the earthquake. The time series shows that the amplitude of the first tsunami wave is larger compared to the amplitude of the trailing waves at most gauges. However, Holberg (Q9) and Port Alice terminal (Q11) experience their largest amplitudes as trailing waves between 8-9 hours after the earthquake. Nerveless, the difference between first wave and the maximum wave is not considerable, and the first wave arrival time may be used for emergency management and preparedness purposes in this case.

Table 7: Tsunami maximum wave amplitudes and arrival times of Qautsino Sound for Alaska-Aleutian current-day scenario at selected numerical gauge points (GP) displayed in Figure 8.

		First wave		Maximum wave	
GP	Location	Arrival time HH:MM	Amplitude (m)	Arrival time HH:MM	Amplitude (m)
Q1	Raft Cove	02:46	1.8	02:46	1.8
Q2	Grant Bay	02:48	1.8	02:48	1.8
Q3	Winter Harbour	02:58	1.2	02:58	1.2
Q4	Quatsino Sound entrance	02:47	0.8	02:47	0.8
Q5	Mahatta River mouth	02:58	1	02:58	1
Q6	Quatsino Hamlet	03:06	0.9	03:06	0.9
Q7	Quatsino Narrows	03:12	1	03:12	1
Q8	Coal Harbour	03:37	0.2	08:37	0.4
Q9	Holberg	03:45	0.3	09:04	0.8
Q10	Port Alice	03:16	1.3	03:16	1.3
Q11	Port Alice terminal	03:24	1.7	08:11	1.8

5.2.2. Tsunami-induced current velocities

The maximum tsunami-induced currents for Alaska event are illustrated in Figure 18. The distribution of tsunami-induced currents along the western coast of Vancouver Island due to the long distance from Alaska source is weaker and more uniform compared to the tsunami currents from Cascadia source when comparing Figures 18 and 12, for Alaska and Cascadia events, respectively. Although the predicted tsunami currents from Alaska event are considerably slower than Cascadia event, the behaviour of the current velocities is similar to those of the Cascadia event within Nootka Sound and Quatsino Sound. For instance, stronger current velocities at shallower, narrower, and constricted waterways and passages are estimated. This indicates that although the tsunami-induced currents of Alaska event are typically slower compared to Cascadia

event, hazardous velocities can still occur. Quantitative tsunami-induced currents of Nootka Sound and Quatsino Sound from Alaska event are discussed below.

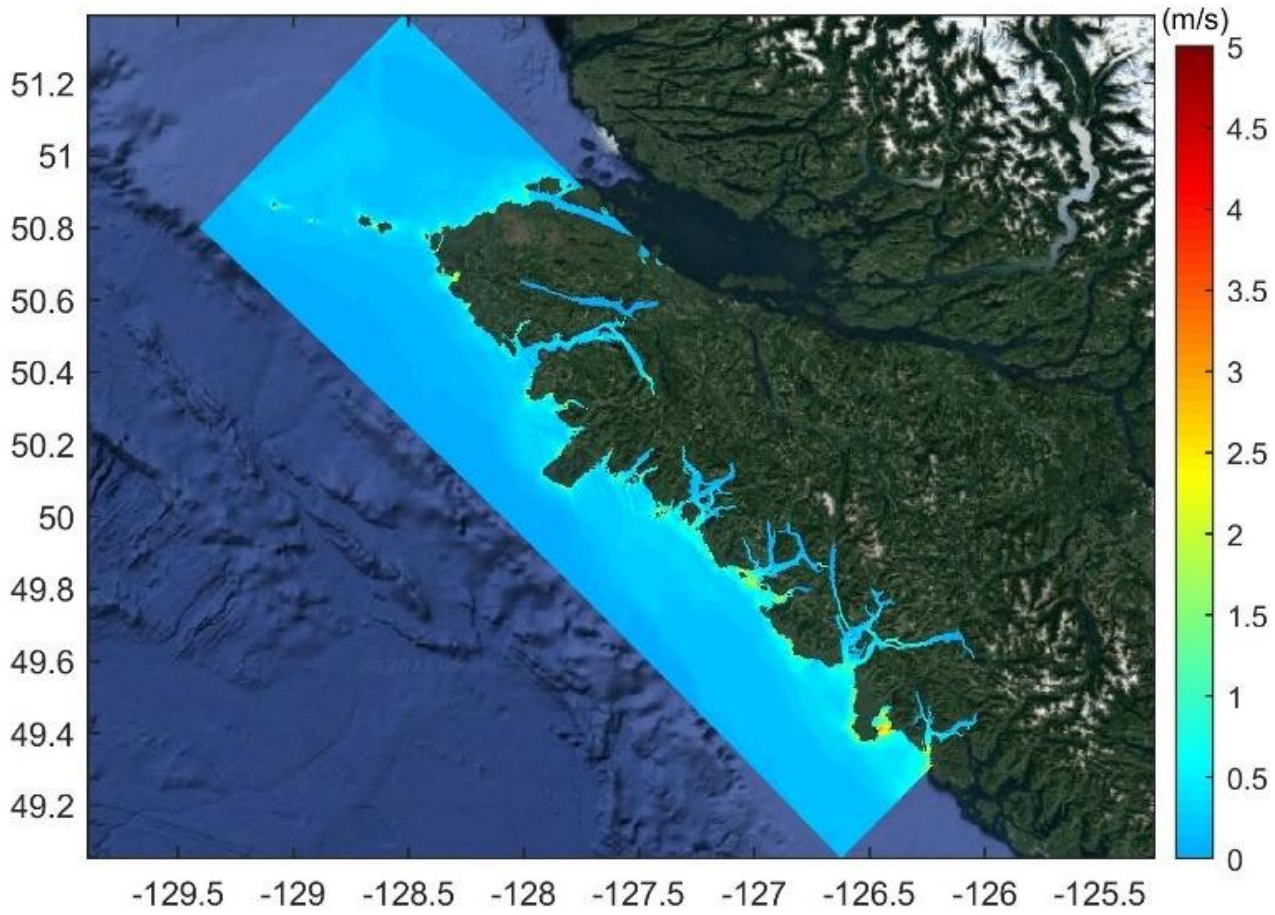

Figure 18: Maximum tsunami current velocities in Northwest Vancouver Island coasts for Scenario2: Alaska-Aleutian current-day resulted from the 60m resolution simulation.

Nootka Sound

The maximum tsunami-induced currents of the Alaska tsunami simulation for Nootka Sound grid is shown in Figure 19. At entrance of Nootka Sound in deep water (e.g., about 100m) the tsunami currents of up to 1 m/s estimated. However, at the sides of Nootka entrance due to its funnel shape and shallow depth the strong currents would reach up to 2 m/s which is consistent with the amplification of wave amplitude at these locations.

Within Nootka Sound tsunami currents of up to 1 m/s is estimated. For instance, in Critter cove, Cougar Creek, and Cheesish. While in Head Bay tsunami currents up to about 2m/s is estimated, as a result of shallower depth.

The tsunami currents are typically stronger close to small island and narrow waterways. For example, in Hanna Channel next to Beligh Island and Williamson Passage in Muchalat Inlet tsunami current of up to 2 m/s is predicted. In deep area of Gold River Terminal (e.g., greater

than 100m) tsunami currents less than 1m/s predicted, however, in shallower water at Gold River waterfront tsunami currents of up to 2 m/s are expected.

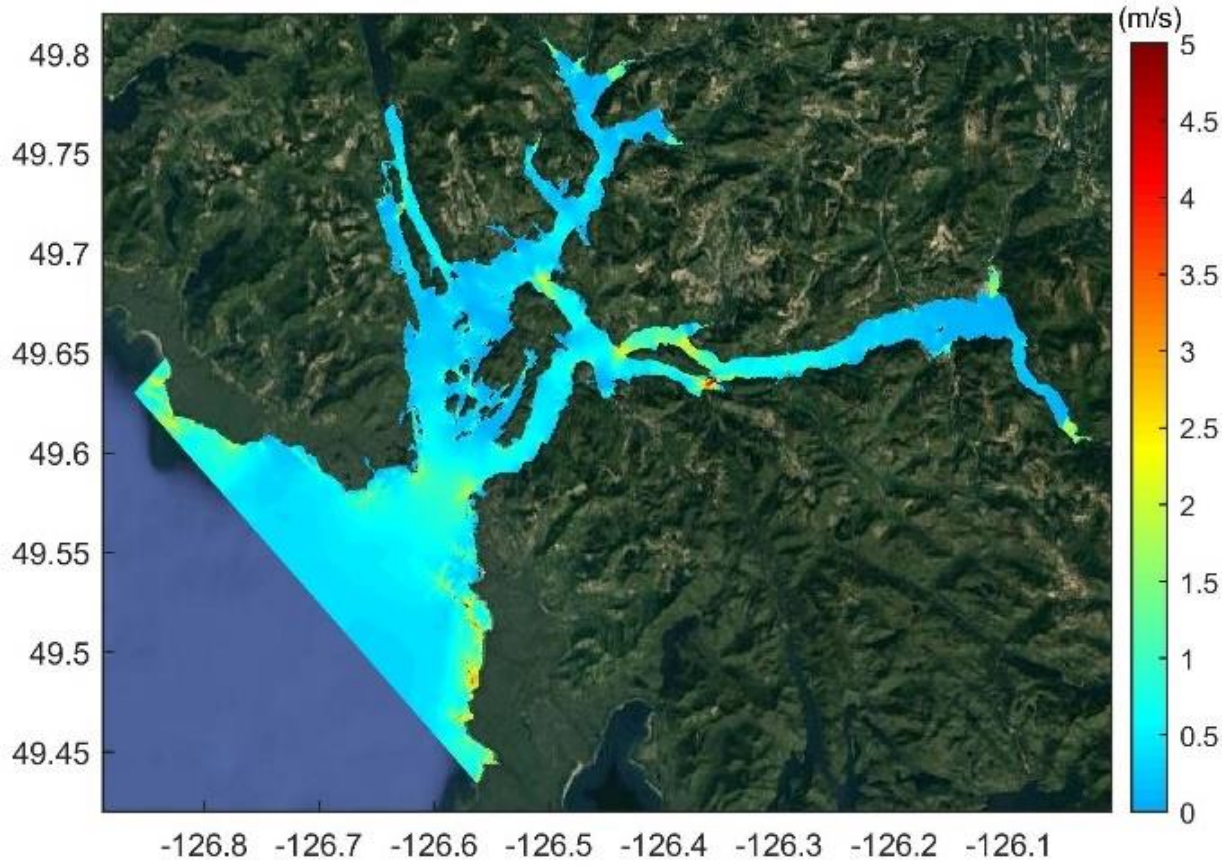

Figure 19: Maximum tsunami current velocities in Nootka Sound for Scenario2: Alaska-Aleutian current-day resulted from the 10m resolution simulation.

Quatsino Sound

The maximum tsunami-induced currents of the Alaska tsunami simulation for Quatsino Sound is shown in Figure 20. On the northwest coast of Vancouver Island from Grant Bay to toward north, the tsunami-induced currents between 1-3 m/s are estimated, where recreational areas such as Raft Cove are located. At the entrance of Quatsino Sound in deeper water (i.e., about 100m) the tsunami currents of about 0.3m/s are estimated. Inside Quatsino Sound tsunami currents are mainly in the range of 0-1 m/s. However, in narrow waterways, channels and close to small islands stronger tsunami currents are expected. For example, in the vicinity of Quattische Island and in Quatsino narrows tsunami currents exceed 2 m/s. Similarly, in Forward Inlet at Winter Harbour South where the geometry is constricted and the depth is relatively shallow (e.g., about 20m) strong currents up to and greater than 3 m/s are predicted.

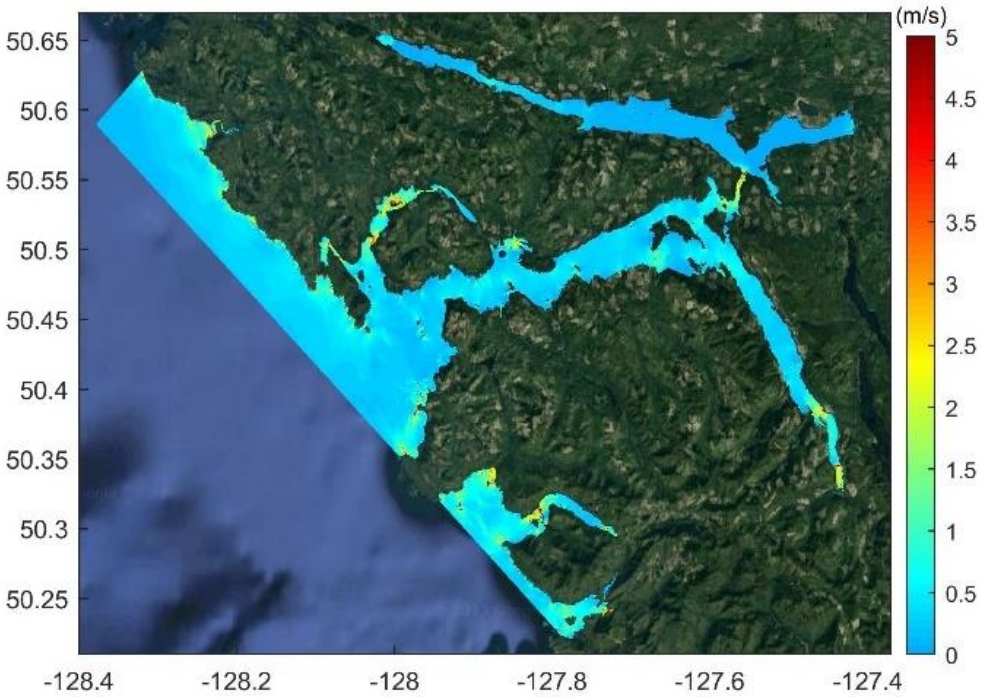

Figure 20: Maximum tsunami current velocities in Quatsino Sound for Scenario2: Alaska-Aleutian current-day resulted from the 10m resolution simulation.

In Holberg Inlet, tsunami-induced currents are small (e.g., less than 0.5 m/s in Coal harbour) and at the end of the inlet at Holberg, it can reach to 1 m/s. In Neroutsos Inlet where the tsunami wave propagates towards Port Alice tsunami-induced currents may exceed 0.5m/s, while in Port Alice terminal with shallower depth the currents would reach up to 3 m/s.

5.3. Future sea level rise

As discussed in Section 4.6, 1.2m of relative Sea Level Rise (SLR) was applied for tsunami modelling for both local and distant tsunami sources. Tsunami modelling results for SLR scenario from Cascadia and Alaska events are presented in Annexes B and C, respectively.

The results show that the inclusion of SLR scenarios (1.2 m) has little influence on the amplitude of the tsunami waves at offshore locations compared to present-day scenario (i.e. no SLR included). Also, the rise in sea level will only weakly change the distribution of tsunami induced currents at offshore locations, although deeper water (SLR scenario) has a tendency to reduce tsunami-induced currents.

Although the SLR does not appear to change the offshore tsunami wave amplitudes substantially, it can cause larger inundation extents and impact communities, specially, in low-lying areas of the region.

For detailed comparison of the water surface elevations from SLR scenario with present-day scenario of the Cascadia and Alaska events, offland numerical gauge points within each high-resolution grid were selected from Table 3. Comparison of the time series of water surface elevation for those gauge points for both Cascadia and Alaska events are presented in Annexes B.3-4, and C.3-4, respectively. The comparison indicates that the tsunami parameters including wave amplitudes and their arrival time for a future tsunami (i.e., 1.2m SLR) are almost similar regardless of minor differences compared to the present-day condition.

5.4. Limitations

The main source of uncertainties in tsunami modelling are due to the tsunami seismic source including uncertainties associated with the structure and vertical displacements of a future subduction zone earthquake scenario.

While Boussinesq models consider physical wave dispersion, they are computationally more demanding compared to SWE models. Furthermore, addressing numerical instabilities in Boussinesq models, which often stems from sharp changes in bathymetry, can be challenging. To address such issue, wave dispersion was neglected in the 10 m simulations, and the modelling was effectively performed based on the nonlinear shallow water equations. As tsunami waves are mainly comprised of long waves, this simplification is not expected to have a considerable influence on the results.

6. SUMMARY

This report was prepared by Ocean Networks Canada (ONC) as part of the Northwest Vancouver Island Tsunami Risk Assessment project for the Strathcona Regional District (SRD) in collaboration with Northwest Hydraulic Consultants (NHC). The project was divided into two phases due to the extensive geographic area of Northwest Vancouver Island. The first phase, completed in 2022, focused on communities in Kyuquot Sound, Tahsis Inlet, and Esperanza Inlet. This report specifically covers phase II of the project and presents tsunami modelling results for Nootka Sound and Quatsino Sound. The study area within phase II includes the communities of Gold River (waterfront), Port Alice, Winter Harbour, Hamlet of Quatsino, Holberg, as well as the Quatsino First Nation and Mowachaht/Muchalaht First Nations.

In this work, high resolution tsunami modelling was performed to assess the tsunami hazard for two earthquake events: Cascadia Subduction Zone (Mw: 9.0) and Alaska Subduction Zone (Mw: 9.2). Both earthquake scenarios were simulated corresponding to current-day sea level and 1.2 m future relative Sea Level Rise (SLR).

The simulations were conducted using FUNWAVE-TVD version 3.4, a fully nonlinear and dispersive Boussinesq wave model, on a nested grid with resolutions of 2 arcminutes, 30 arc-seconds, 240m, 60m, and 10m. Digital elevation models (DEMs) were developed for the study area at resolutions of 240m, 60m, and 10m, relative to the Canadian Geodetic Vertical Datum CGVD2013, using various available or collected bathymetric and topographic data sources. All simulations were performed at the High High Water Mean Tide (HHWMT) level, which was determined to be 1.5m above the CGVD2013 level.

The results indicated that tsunami waves generated by the Cascadia earthquake event are larger, particularly within Nootka Sound, and have a more significant impact on the study area compared to the Alaska tsunami. The first tsunami wave would reach most study sites between 30 min to 1 hour for the Cascadia earthquake and between 2h:46min to 3h:30min for the Alaska earthquake. The following sections provide a summary of the modelling results for the study areas during the Cascadia and Alaska events.

Cascadia Subduction zone

The maximum tsunami wave amplitudes within Nootka Sound range from 2-4 m in most areas, with amplification occurring towards the end of the inlets. The Gold River waterfront and Head Bay encounter elevated wave amplitudes, reaching up to 6m and exceeding 8 m, respectively. The first tsunami wave arrives at Nootka Sound communities in less than an hour from the earthquake.

In Quatsino Sound, tsunami wave amplitudes vary between 1-2 m, while along the open coasts of the Northwest of Vancouver Island, they range from 2-3 m. Semi-enclosed bays and inlets experience increased amplitudes such as Grant Bay, Winter Harbour and Port Alice Terminal having maximum amplitudes of up to 3 m.

Tsunami-induced currents are stronger from Brooks Peninsula towards Nootka Sound, exceeding 5 m/s at the open coast of Nootka Sound entrance, while currents at Quatsino Sound entrance are less than 2 m/s. Within Nootka Sound, currents range from 1-2 m/s, with stronger velocities exceeding 5 m/s in some of the narrower waterways and passages. In Quatsino Sound, currents are generally slower, ranging from 0-1 m/s, with stronger currents exceeding 5 m/s in specific areas like Quatsino Narrows and Winter Harbour.

Alaska-Aleutian Subduction Zone

The maximum tsunami wave amplitudes along the western coast of Vancouver Island range from 1-2 m. Within Nootka Sound, the maximum wave amplitudes are generally around 1 m, but they amplify at the Muchalat Inlet up to 4 m and Tlupana Inlet up to 2 m. The first tsunami wave is expected to reach Nootka Sound communities within 3-4 hours.

In Quatsino Sound, the maximum wave amplitudes predicted up to 1 m, but they increase in semi-enclosed bays and inlets such as Grant Bay and Neroutsos Inlet up to and above 2 m. The first tsunami wave would reach most Quatsino Sound communities approximately 3 hours after the Alaska event, and the initial peak wave is larger compared to trailing waves in most locations. Tsunami-induced currents along the coast are weaker for the Alaska event compared to the Cascadia event, but they still pose hazards in areas with shallower depth, narrower topography, and constricted passages.

Within Nootka Sound and Quatsino Sound, tsunami-induced currents range from 0-1 m/s, but higher velocities are estimated in specific locations such as William passage in Nootka Sound and Quatsino narrows and Winter Harbour in Quatsino Sound.

The study also suggests that sea level rise scenarios may not significantly alter tsunami wave amplitudes offshore and near the shoreline, but they can increase wave run-up and inundation extents during future tsunamis.

REFERENCES

AECOM 2013. Modelling of Potential Tsunami Inundation Limits and Run-Up, Capital Regional District, Project No. 6024 2933, 36 p.

Atwater, B. F., Nelson, A. R., Clague, J. J., Carver, G. A., Yamaguchi, D. K., Bobrowsky, P. T., ... & Reinhart, M. A. (1995). Summary of coastal geologic evidence for past great earthquakes at the Cascadia Subduction Zone. *Earthquake spectra*, *11*(1), 1-18.

Barua, D. K., Allyn, N. F., & Quick, M. C. (2007). Modelling tsunami and resonance response of Alberni inlet, British Columbia. In *Coastal Engineering 2006: (In 5 Volumes)* (pp. 1590-1602).
Benson, B.E., Grimm, K.A., Clague, J. J., 1997. Tsunami Deposits beneath Tidal Marshes on Northwestern Vancouver Island, British Columbia. Quaternary Research, 48, 192-204.

Fisheries and Oceans Canada (2023). *Canadian Tide & Current Tables. Vol. 6, Discovery Passage and West Coast of Vancouver Island*.

Clague, J. J., Bobrowsky, P. T., & Hutchinson, I. (2000). A review of geological records of large tsunamis at Vancouver Island, British Columbia, and implications for hazard. *Quaternary Science Reviews*, *19*(9), 849-863.

Clague, John J., and Peter T. Bobrowsky. Tsunami deposits beneath tidal marshes on Vancouver Island, British Columbia. *Geological Society of America Bulletin* 106.10 (1994): 1293-1303.

Dunbar, D., LeBlond, P.H., Murty, T.S., 1989. Maximum tsunami amplitudes and associated currents on the coast of British Columbia. Science of Tsunami Hazards 7, 3-44

Dunbar, D., LeBlond, P.H., Murty, T.S., 1991. Evaluation of tsunami amplitudes for the Pacific coast of Canada. Progress in Oceanography 26, 115-177.

Dunbar, P.K., Weaver, C.S. 2008. U.S. states and territories national tsunami hazard assessment - Historical record and sources for waves: Technical Report, National Oceanic and Atmospheric Administration and U.S. Geological Survey, 59 pp.

Fine, I.V., Thomson, R.E, 2020. Numerical Simulation of a Cascadia Subduction Zone Tsunami with Application to Boundary Bay in the Southern Strait of Georgia, Institute of Ocean Sciences, Fisheries and Oceans Canada.

Fine, I.V., Thomson, R. E., Lupton, L. M., & Mundschutz, S. 2018a. Numerical Modelling of a Cascadia Subduction Zone Tsunami at the Canadian Coast Guard Base in Victoria, British Columbia. Fisheries and Oceans Canada= Pêches et océans Canada.

Fine I.V., Thomson, R.E., Lupton, L.M., and Mundschutz, S. 2018b. Numerical modelling of a Cascadia Subduction Zone tsunami at the Canadian Coastal Base at Seal Cove, Prince Rupert, British Columbia

Gao, D., Wang, K., Insua, T. L., Sypus, M., Riedel, M., Sun, T. 2018. Defining megathrust tsunami source scenarios for northernmost Cascadia. *Natural Hazards*. 94: 445-469. doi:10.1007/s11069-018-3397-6.

Geist, L. G., Parsons, T. 2006. Probabilistic analysis of tsunami hazards. *Natural Hazards*. 37: 277-314. doi:10.1007/s11069-005-4646-z.

Goda, K., 2022 Stochastic source modeling and tsunami simulations of Cascadia subduction earthquakes for Canadian Pacific coast. Coastal Engineering Journal, 64(4), 575-596. doi: 10.1080/21664250.2022.2139918.

Goldfinger, C., Nelson, C. H., Morey, A. E., Johnson, J. E., Patton, J. R., Karabanov, E., Gutierrez-Pastor, J., Eriksson, A. T., Gracia, E., Dunhill, G., Enkin, R. J. 2012. Turbidite event history: Methods and implications for Holocene paleoseismicity of the Cascadia Subduction Zone. U.S. Geological Survey Professional Paper, 1661, 170.

Grilli, S.T., Harris, J.C., Tajalli Bakhsh, T.S., Masterlark, T.L., Kyriakopoulos, C., Kirby, J.T. and Shi, F. (2012) 'Numerical Simulation of the 2011 Tohoku Tsunami Based on a New Transient FEM Co-seismic Source: Comparison to Far- and Near-Field Observations', Pure and Applied Geophysics, 170(6), pp. 1333-1359.

Grilli S.T., O'Reilly C., Harris J.C., Tajalli-Bakhsh T., Tehranirad B., Banihashemi S., Kirby J.T., Baxter C.D.P., Eggeling T., Ma G. and F. Shi 2015. Modelling of SMF tsunami hazard along the upper US East Coast: Detailed impact around Ocean City, MD. Natural Hazards, 76(2), 705-746, doi: 10.1007/s11069-014-1522-8

Hebenstreit, G. T., & Murty, T. S. (1989). Tsunami amplitudes from local earthquakes in the pacific northwest region of North America part 1: The outer coast. *Marine Geodesy*, *13*(2), 101-146.

Horrillo, J., Grilli, S. T., Nicolsky, D., Roeber, V., Zhang, J. 2014. Performance benchmarking tsunami operational models for NTHMP's inundation mapping activities. *Pure and Applied Geophysics*. 172: 869-884, doi: 10.1007/s00024-014-0891-y.

Imamura, F., Shuto, N. and Goto, C. (1988). Numerical simulations of the transoceanic propagation of tsunamis, Proc. 6th Congress Asian and Pacific Regional Division, IAHR, Japan, 265-272.

Intergovernmental Oceanographic Commission. Fourth Edition. Tsunami Glossary, 2019. Paris, UNESCO. IOC Technical Series, 85. (English, French, Spanish, Arabic, Chinese) (IOC/2008/TS/85 rev.4).

James, T. S., Robin, C., Henton, J. A., & Craymer, M. 2021. Relative sea-level projections for Canada based on the IPCC Fifth Assessment Report and the NAD83v70VG national crustal velocity model.

Johnson, J. M., Satake, K., Holdahl, S. R., Sauber, J. 1996. The 1964 Prince William Sound earthquake: Joint inversion of tsunami and geodetic data. *Journal of Geophysical Research*. 101(B1): 523-532.

Kirby, J. T., Shi, F., Tehranirad, B., Harris, J. C., Grilli, S. T. 2013. Dispersive tsunami waves in the ocean: Model equations and sensitivity to dispersion and Coriolis effects. Ocean Modelling. 62: 39-55. doi:10.1016/j.ocemod.2012.11.009.

Kirby J, Wei G, Chen Q, Kennedy A, Dalrymple R. 1998. FUNWAVE 1.0, fully nonlinear Boussinesq wave model documentation and users manual. Tech. Rep. Research Report No. CACR-98-06, Center for Applied Coastal Research, University of Delaware.

Li, L., Switzer, A. D., Wang, Y., Chan, C. H., Qiu, Q., & Weiss, R. (2018). A modest 0.5-m rise in sea level will double the tsunami hazard in Macau. *Science advances*, *4*(8), eaat1180.

Liu, P. L.-F., Cho, Y.-S., Yoon, S. B. and Seo, S. N., (1994). Numerical simulations of the 1960 Chilean tsunami propagation and inundation at Hilo, Hawaii, Progress in Prediction. Disaster Prevention and Warning, Kluwer Academic Publishers, 99-115.

Ludwin, R.S., Dennis, R., Carver, D., McMillan, A.D., Losey, R., Clague, J., Jonientz-Trisler, C., Bowechop, J., Wray, J., and James, K., 2005. Dating the 1700 Cascadia earthquake: Great coastal earthquakes in Native stories: Seismological Research Letters, v. 76, no. 2, p. 140–148, doi: 10.1785/gssrl.76.2.140.

Lynett P, Wu T-R., Liu PL-F. 2002. Modelling wave runup with depth-integrated equations. Coastal Engineering 46(2), 89–107.

Ma, G., Shi, F., and Kirby, J. T., 2012, "Shock-capturing non-hydrostatic model for fully dispersive surface wave processes", Ocean Modelling, 43, 22-35. doi:10.1016/j.ocemod.2011.12.002

Murty, T. S., & Hebenstreit, G. T. (1989). Tsunami amplitudes from local earthquakes in the pacific Northwest region of north America Part 2: Strait of Georgia, Juan de Fuca Strait, and Puget Sound. *Marine Geodesy*, *13*(3), 189-209.

Nelson, A. R., Briggs, R. W., Dura, T., Engelhart, S. E., Gelfenbaum, G., Bradley, L-A., Forman, S. L., Vane, C. H., Kelley, K. A. 2015. Tsunami recurrence in the eastern Alaska-Aleutian arc: A Holocene stratigraphic record from Chirikof Island, Alaska. *Geosphere*. 11: 1172-1203. doi:10.1130/GES01108.1

Nemati, F., Grilli, S.T., Ioualalen, M., Boschetti, L., Larroque, L. and J. Trevisan, 2018. High-resolution coastal hazard assessment along the French Riviera from co-seismic tsunamis generated in the Ligurian fault system. Natural Hazards, pp. 1-34, doi.org/10.1007/s11069-018-3555-x

NTHMP, 2010. Tsunami Modelling and Mapping: Guidelines and Best Practices, Part I: Tsunami Inundation Modelling, National Tsunami Hazard Mitigation Program. Available at: https://nws.weather.gov/nthmp/documents/1inundationmodellingguidelines.pdf (Accessed: 28/09/2021)

ONC, 2019. Co-seismic tsunami hazard assessment for Prince Rupert. Prepared by Ocean Networks Canada in collaboration with Northwest Hydraulic Consultants for the City of Prince Rupert.

ONC, 2022a. Canadian Safety and Security Program (CSSP) Coastal Flood Mitigation Canada Project Boundary Bay, BC Case Study
ONC, 2022b. Co-seismic Tsunami Hazard Assessment for Northwest Vancouver Island – Phase I.

ONC, 2023a. Co-seismic Tsunami Hazard Assessment for Haida Gwaii.

ONC, 2023b. Northwest Vancouver Island Tsunami Risk Assessment - Phase II. Digital Elevation Models Metadata Report.

Rabinovich, A. B., Thomson, R. E., Krassovski, M. V., Stephenson, F. E., & Sinnott, D. C. (2019). Five great tsunamis of the 20th century as recorded on the coast of British Columbia. *Pure and Applied Geophysics*, *176*(7), 2887-2924.

Sandwell, A. (2011). Climate Change Adaption Guildeines for Sea Dikes and Coastal Flood Hazard Use–Sea Dikes Guidelines. *Report prepared for Ministry of the Environment*, *19*.

Schambach L, Grilli ST, Kirby JT, Shi F (2018) Landslide tsunami hazard along the upper US East Coast: effects of slide rheology, bottom friction, and frequency dispersion. Pure Appl Geophys. https ://doi.org/10.1007/s0002 4-018-1978-7.

Shelby, M., Grilli, S. T. and Grilli, A. R., 2016. Tsunami hazard assessment in the Hudson River Estuary based on dynamic tsunami-tide simulations. Pure and Applied Geophysics, 173(12), 3,999-4,037, doi:10.1007/s00024-016-1315-y

Shi, F., Kirby, J. T., Harris, J. C., Geiman, J. D., Grilli, S. T. 2012. A high-order adaptive time-stepping TVD solver for Boussinesq modelling of breaking waves and coastal inundation. Ocean Modelling. 43-44: 36:51. doi:10.1016/j.ocemod.2011.12.004.

Suito, H., Freymueller, J. T. 2009. A viscoelastic and afterslip postseismic deformation model for the 1964 Alaska earthquake. *Journal of Geophysical Research*. 114, B11404, doi:10.1029/2008JB005954.

Suleimani, E.N., Nicolsky, D.J., and Koehler, R.D. (2013). Tsunami Inundation Maps of Sitka, Alaska. Report of Investigations 2013-3, State of Alaska, Department of Natural Resources, Division of Geological and Geophysical Surveys, Fairbanks, AK, 76 p., 1 sheet, scale 1:250,000. doi: 10.14509/26671.

Suleimani, E., & Freymueller, J. T. (2020). Near-field modelling of the 1964 Alaska tsunami: The role of splay faults and horizontal displacements. *Journal of Geophysical Research: Solid Earth*, *125*(7), e2020JB019620.

Titov, V.V. and Synolakis, C. E. (1998). Numerical modelling of tidal wave runup, J. Waterway, Port, Coastal and Ocean Eng., ASCE, 124(4), 157-171.

Wei, G., Kirby, J.T., Grilli, S.T., and Subramanya, R., 1995. A fully nonlinear Boussinesq model for surface waves: Part I. Highly nonlinear unsteady waves, Journal of Fluid Mechanics, 294, 7192.

Wigen, S. O., White, W. R. H. 1964. Tsunami of March 27-29, 1964: West coast of Canada. Canada Department of Mines and Technical Surveys. 13 pp.

Wronna, M., Omira, R., Baptista, M. A. 2015. Deterministic approach for multiple-source tsunami hazard assessment for Sines, Portugal. *Natural Hazards and Earth System Sciences*. 15: 2557-2568, doi: 10.5194/nhess-15-2557-2015.

Yamazaki Y., Cheung, K. F. and Kowalik, Z. 2010 Depth- integrated, non-hydrostatic model with grid nesting for tsunami generation, propagation, and runup. International Journal for Numerical Methods in Fluids. https://doi.org/10.1002/fld.2485

ANNEXE A: TIME SERIES OF WATER SURFACE ELEVATION

A.1 Cascadia subduction zone, Nootka Sound

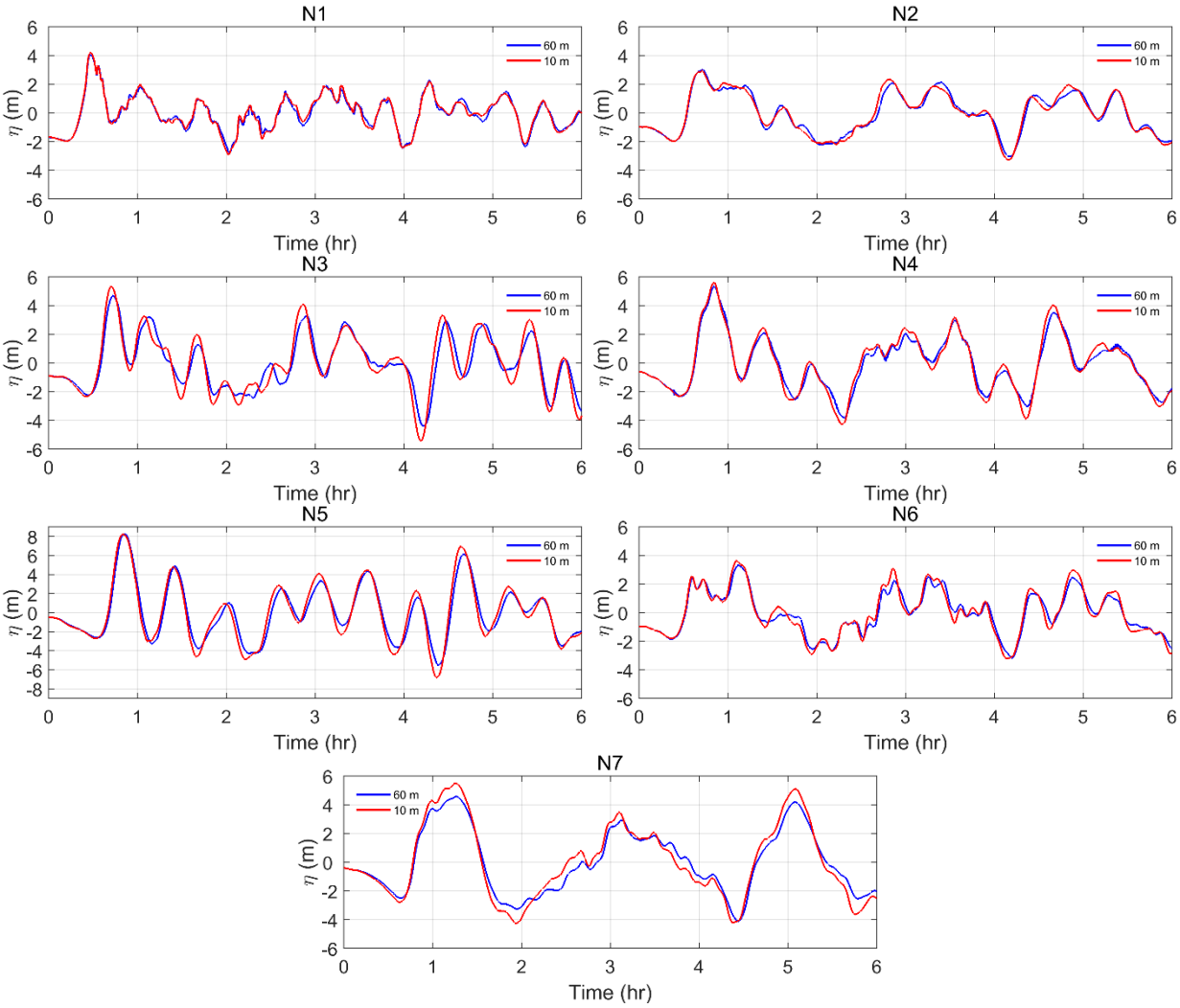

Figure A.1. Time series of water surface elevation for selected numerical gauge points of Nootka grid from Cascadia tsunami source using 60m and 10m resolutions. The water surface elevation (η) is with respect to HHWMT.

A.2 Cascadia subduction zone, Quatsino Sound

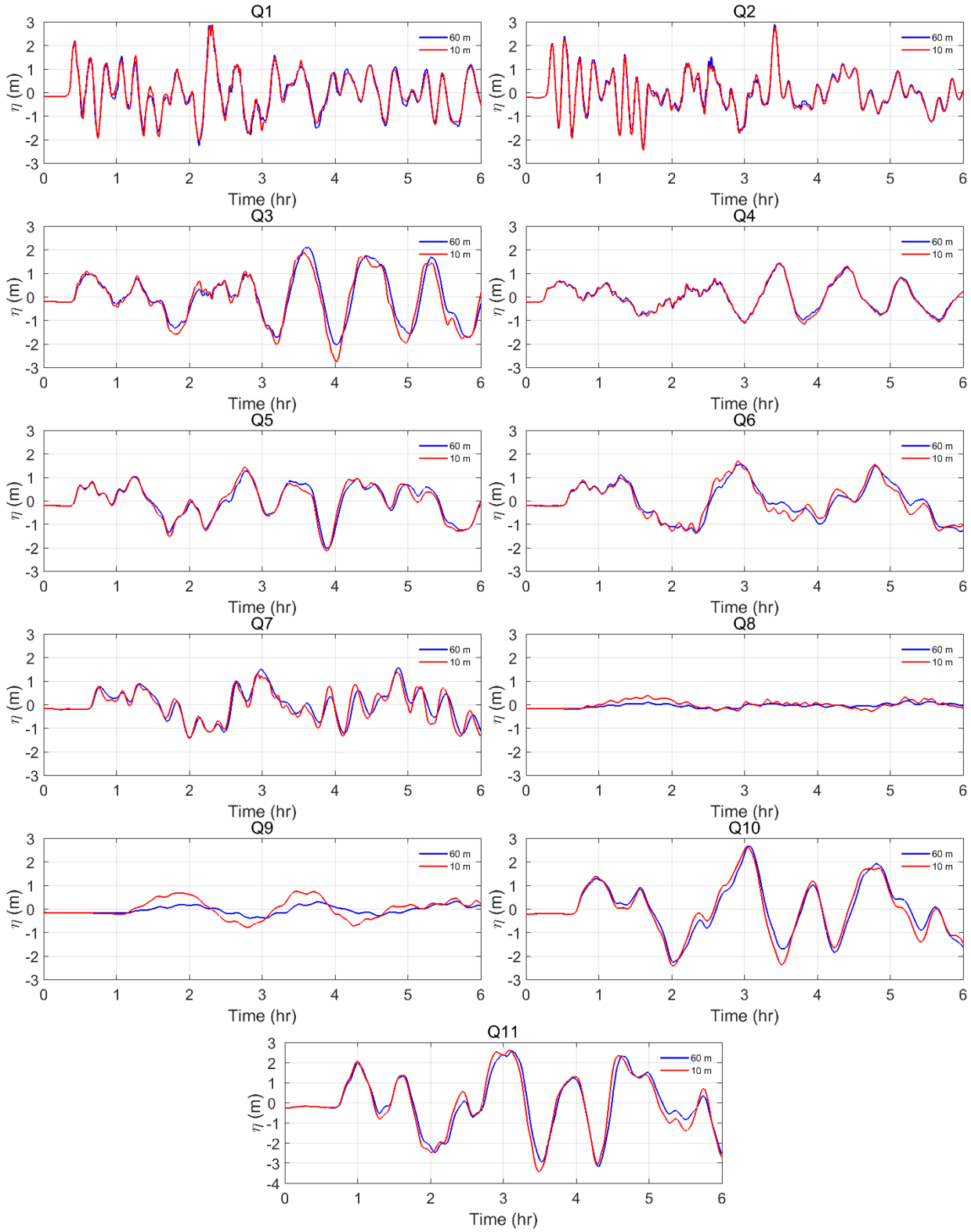

Figure A.2. Time series of water surface elevation for selected numerical gauge points of Quatsino grid from Cascadia tsunami source using 60m and 10m resolutions. The water surface elevation (η) is with respect to HHWMT.

A.3 Alaska-Aleutian subduction zone, Nootka Sound

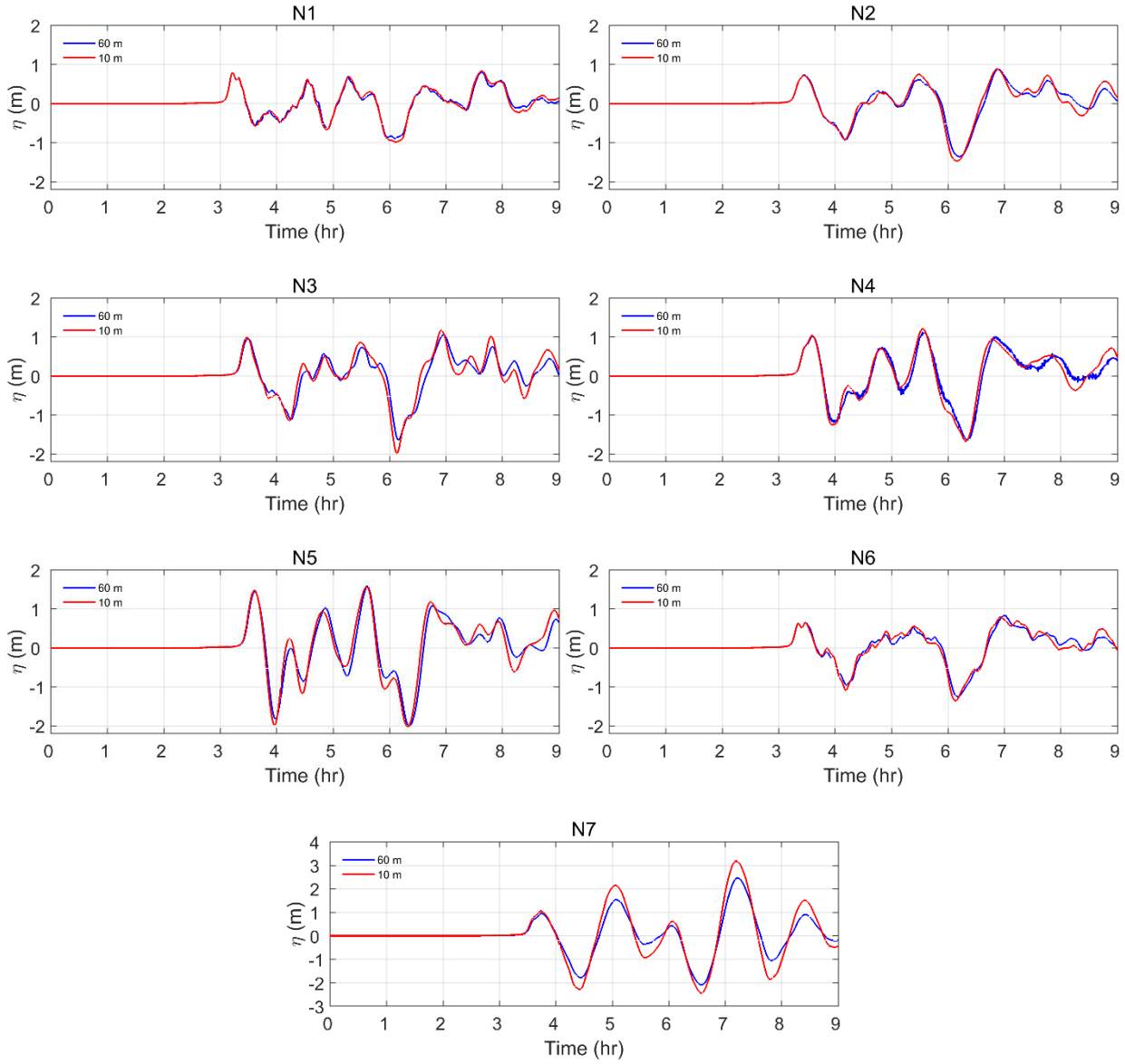

Figure A.3. Time series of water surface elevation for selected numerical gauge points of Nootka grid from Alaska tsunami source using 60m and 10m resolutions. The water surface elevation (η) is with respect to HHWMT.

A.4 Alaska-Aleutian subduction zone, Quatsino Sound

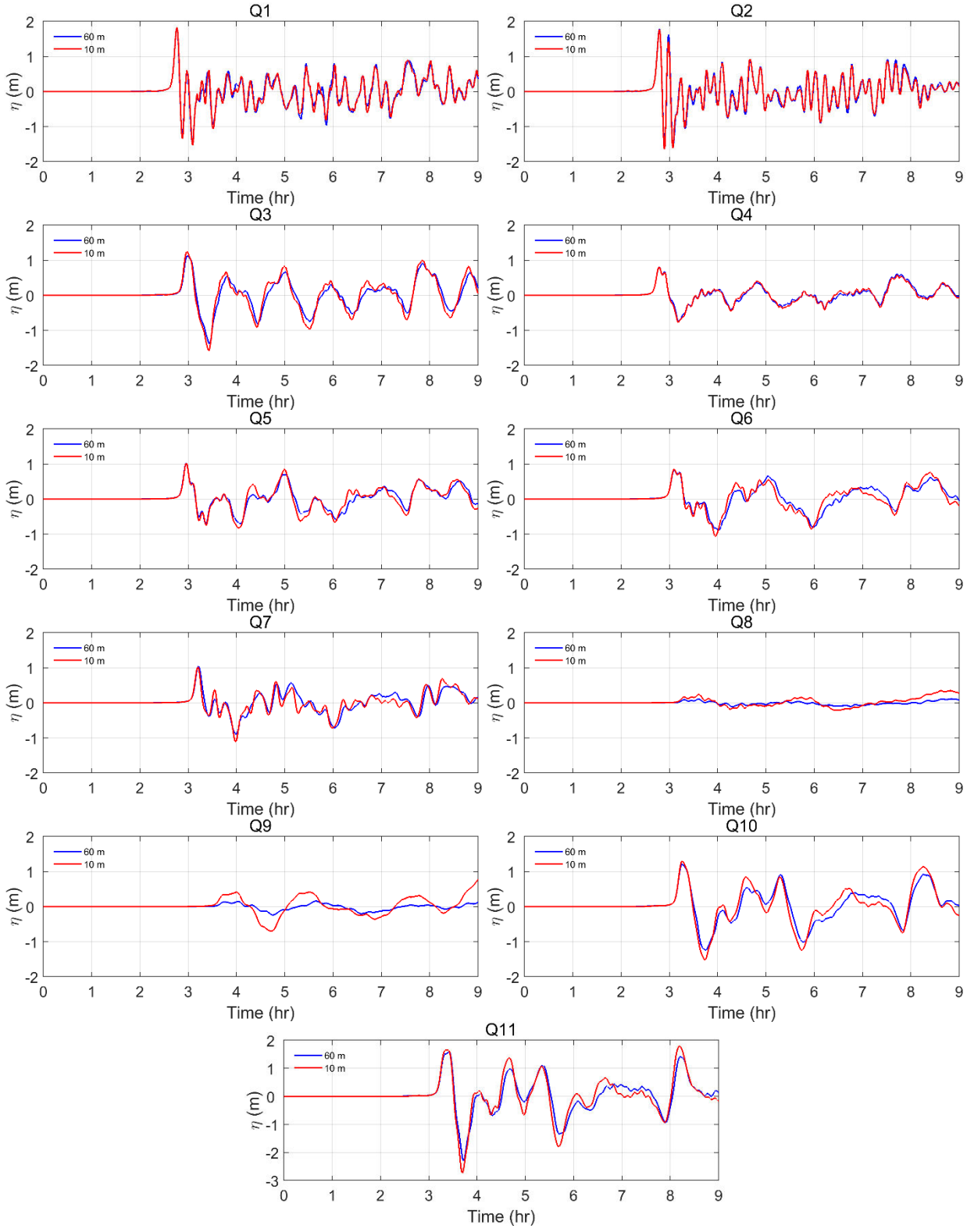

Figure A.4. Time series of water surface elevation for selected numerical gauge points of Quatsino grid from Alaska tsunami source using 60m and 10m resolutions. The water surface elevation (η) is with respect to HHWMT.

ANNEXE B: CASCADIA SUBDUCTION ZONE, SEA LEVEL RISE RESULTS

B.1 Tsunami wave amplitude

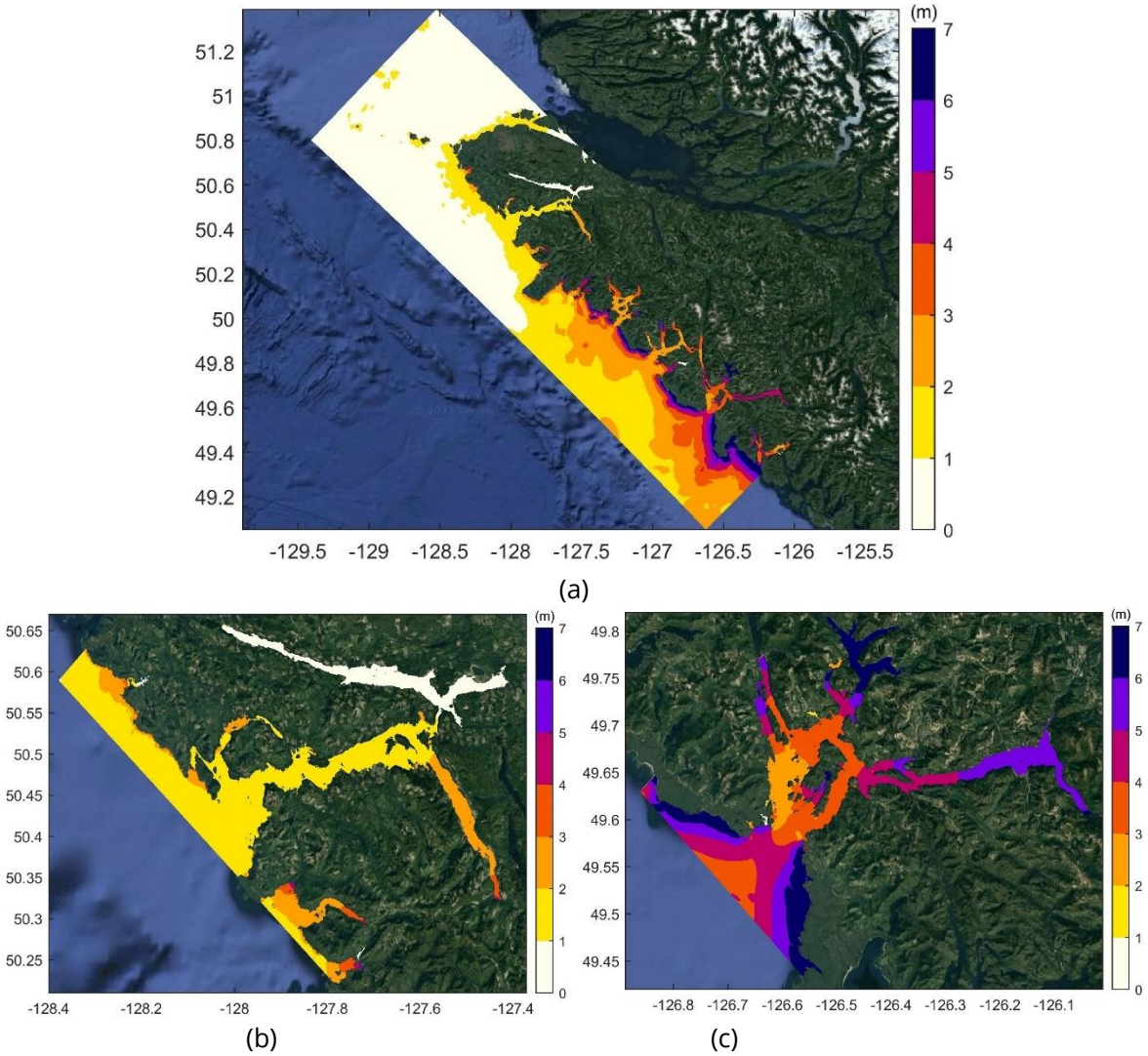

Figure B1: Maximum tsunami wave amplitudes for Scenario3: Cascadia Subduction Zone with 1.2m SLR a) 60 m resolution grid, b) 10m resolution grid of Quatsino, and c) 10m resolution grid of Nootka.

B.2 Tsunami-induced currents

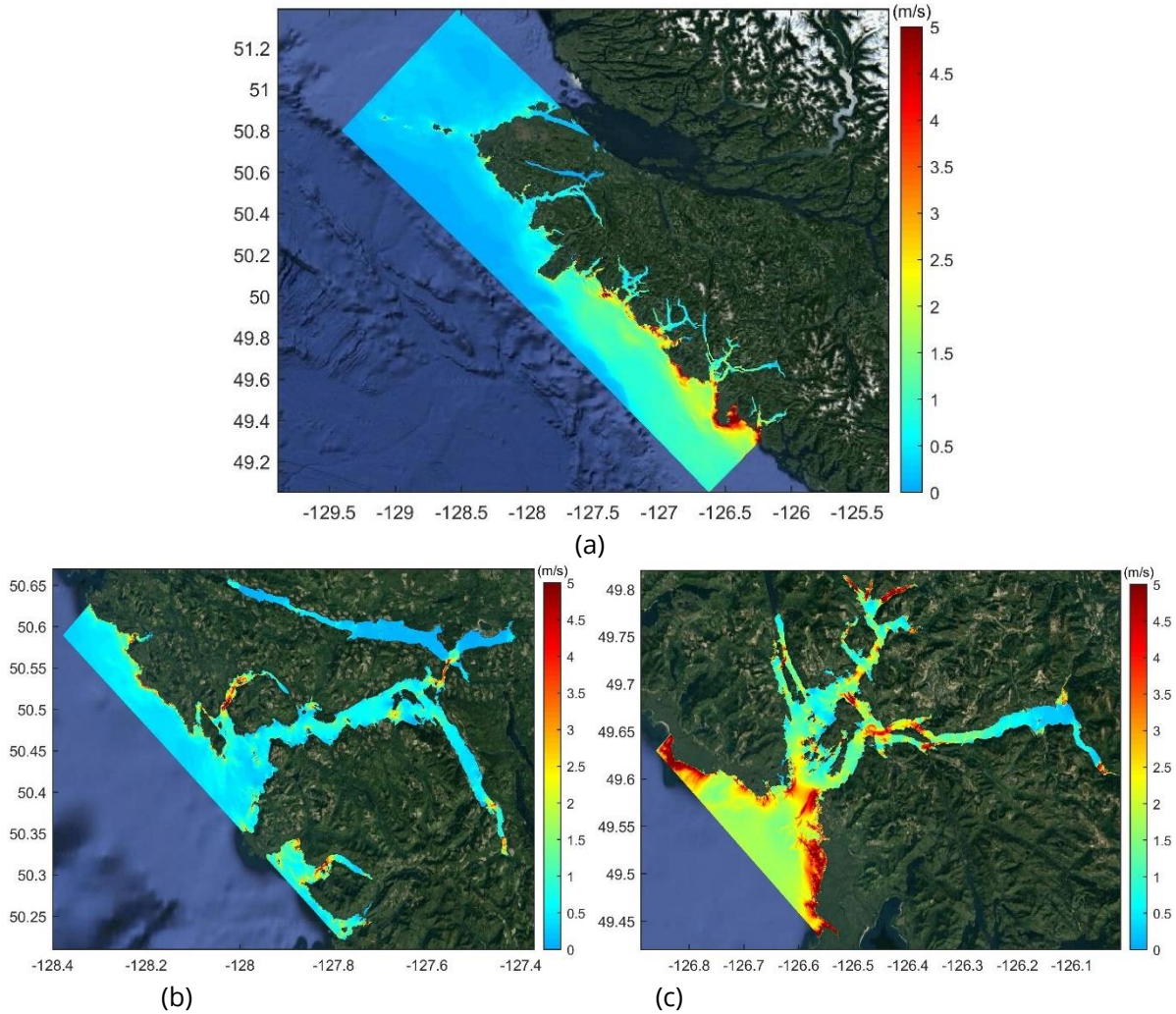

Figure B2: Maximum tsunami current velocities for Scenario3: Cascadia Subduction Zone with 1.2m SLR a) 60 m resolution grid, b) 10m resolution grid of Qautsino, and c) 10m resolution grid of Nootka.

B.3 Time series of water surface elevation, of Nootka Sound (0m, 1.2m SLR comparison)

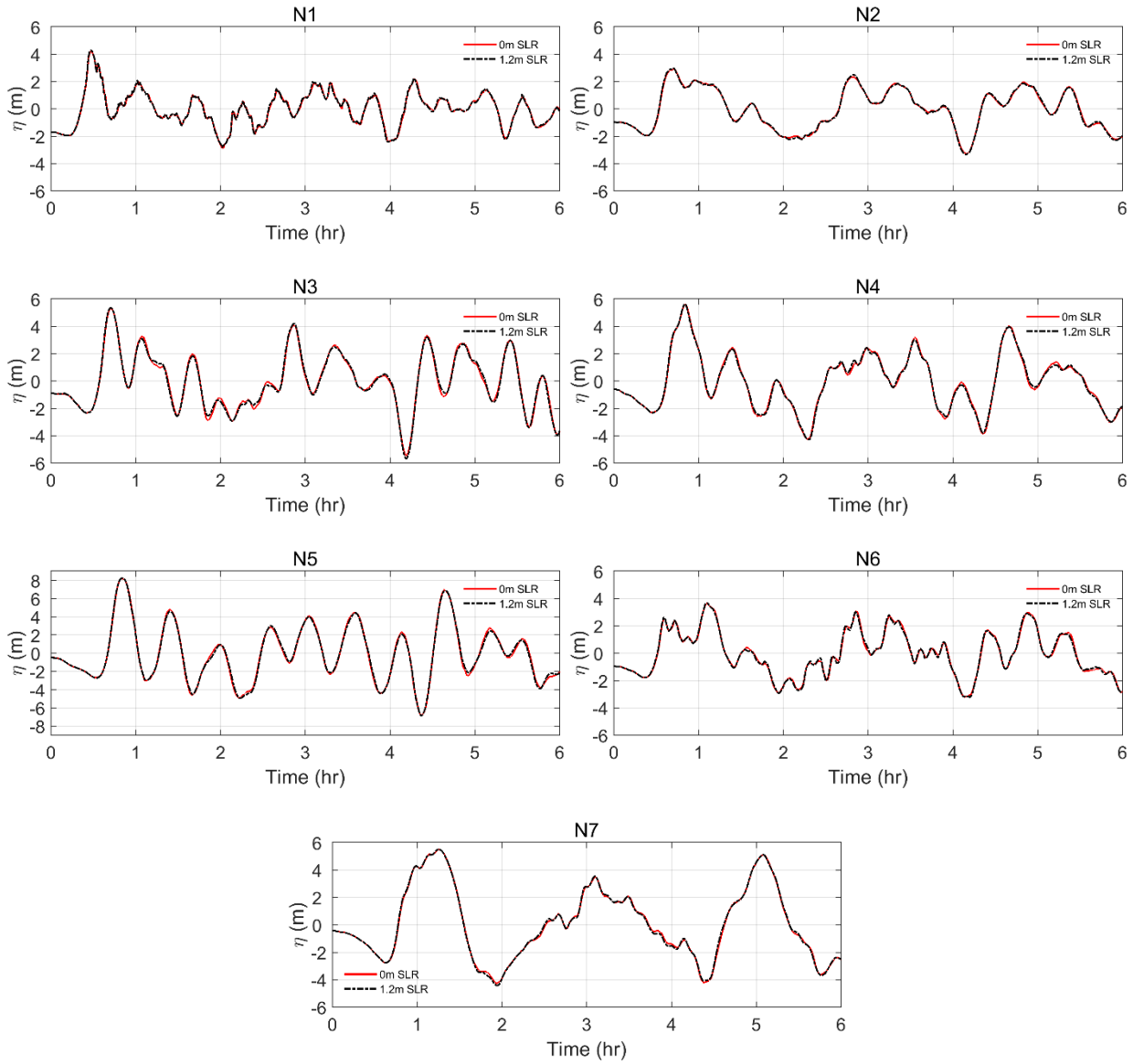

Figure B.3: Time series of water surface elevation for selected numerical gauge points of Nootka grid for present-day (0m SLR) and future scenario (1.2m SLR) from Cascadia tsunami source. The water surface elevation (η) is with respect to HHWMT.

B.4 Time series of water surface elevation, of Quatsino Sound (0m, 1.2m SLR comparison)

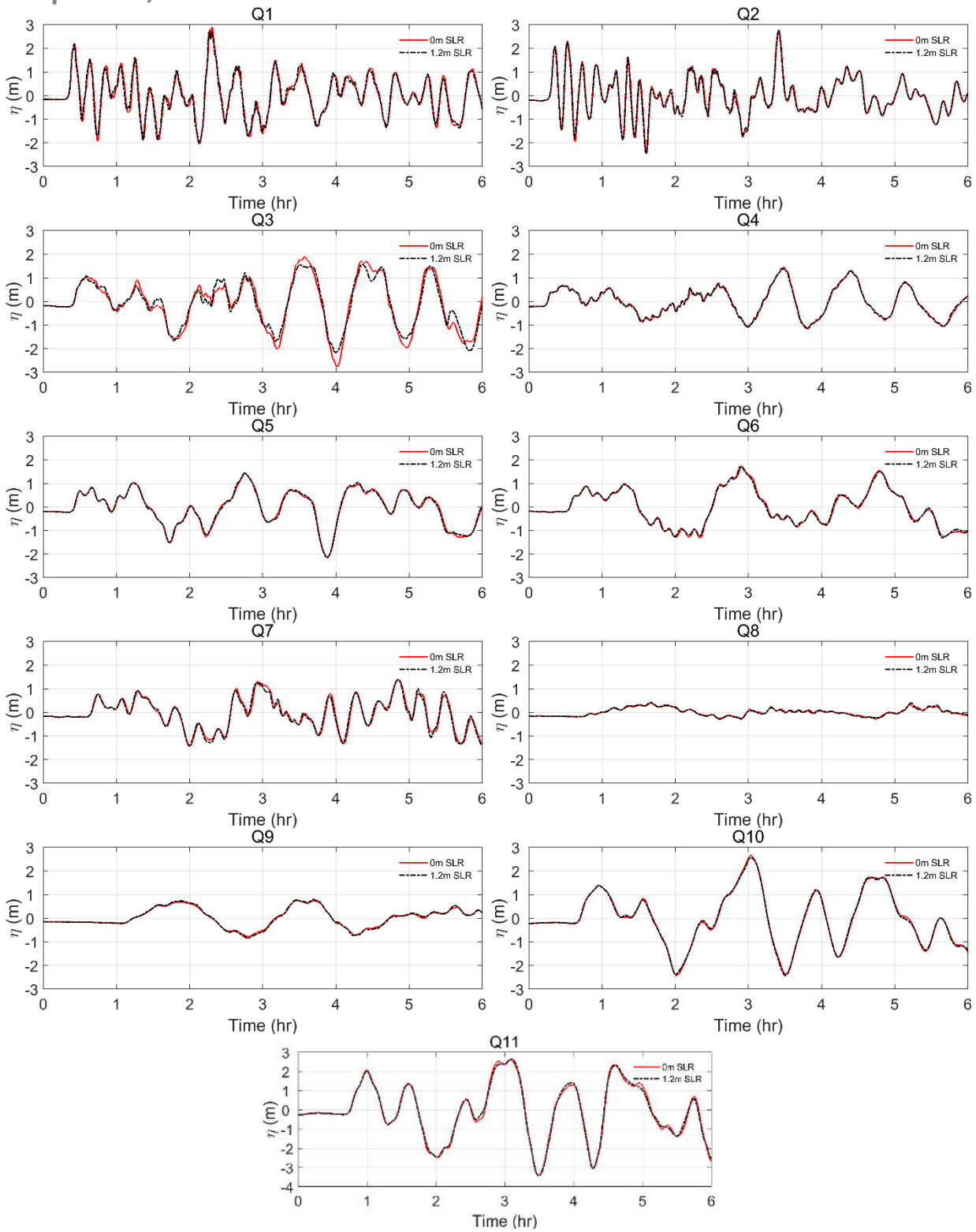

Figure B.4: Time series of water surface elevation for selected numerical gauge points of Quatsino grid for present-day (0m SLR) and future scenario (1.2m SLR) from Cascadia tsunami source. The water surface elevation (η) is with respect to HHWMT.

ANNEXE C: ALASKA-ALEUTIAN SUBDUCTION ZONE, SEA LEVEL RISE RESULTS

C.1 Tsunami wave amplitude

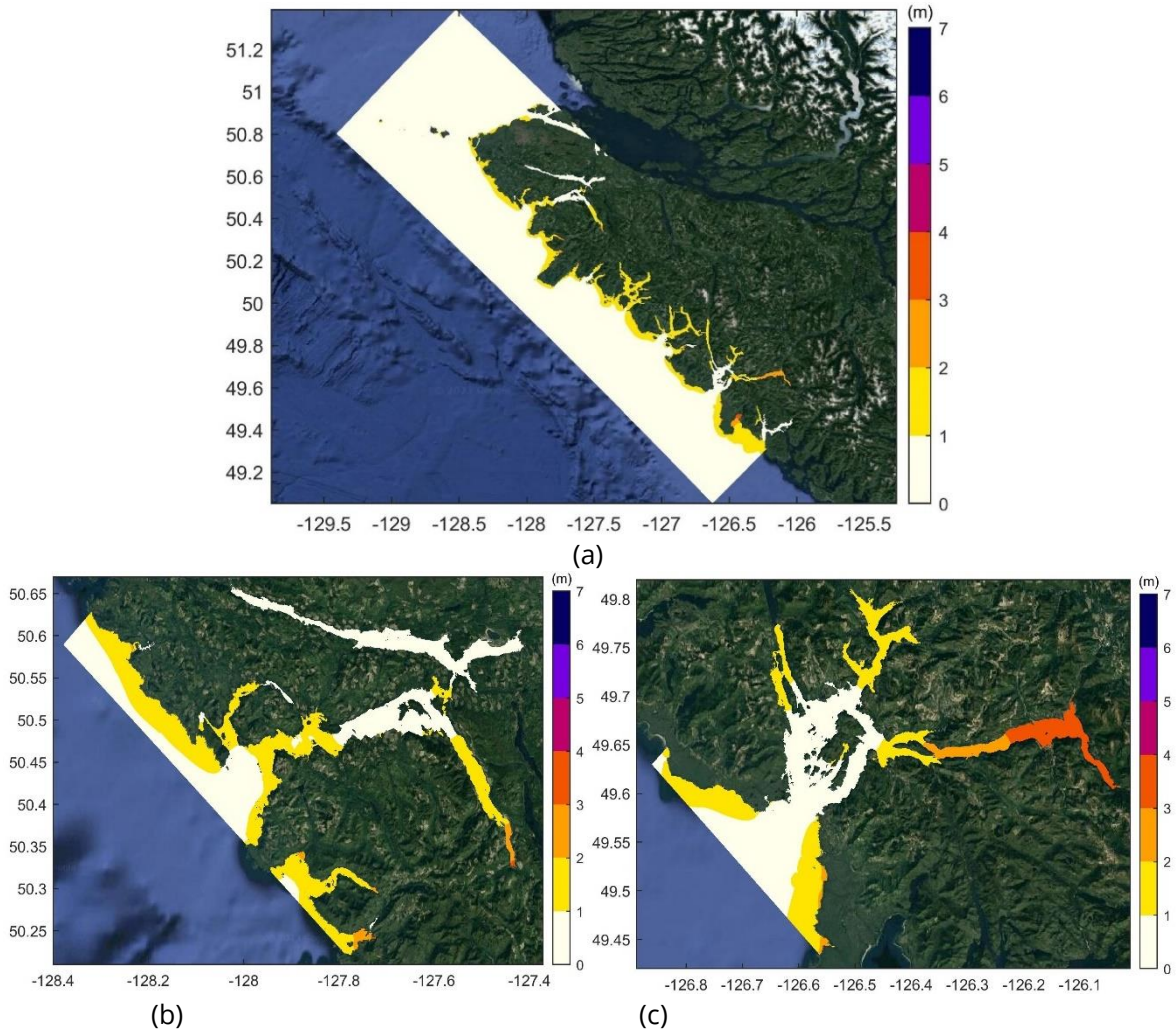

Figure C1: Maximum tsunami wave amplitudes for Scenario4: Alaska-Aleutian Subduction Zone with 1.2m SLR a) 60 m resolution grid, b) 10m resolution grid of Quatsino, and c) 10m resolution grid of Nootka.

C.2 Tsunami-induced currents

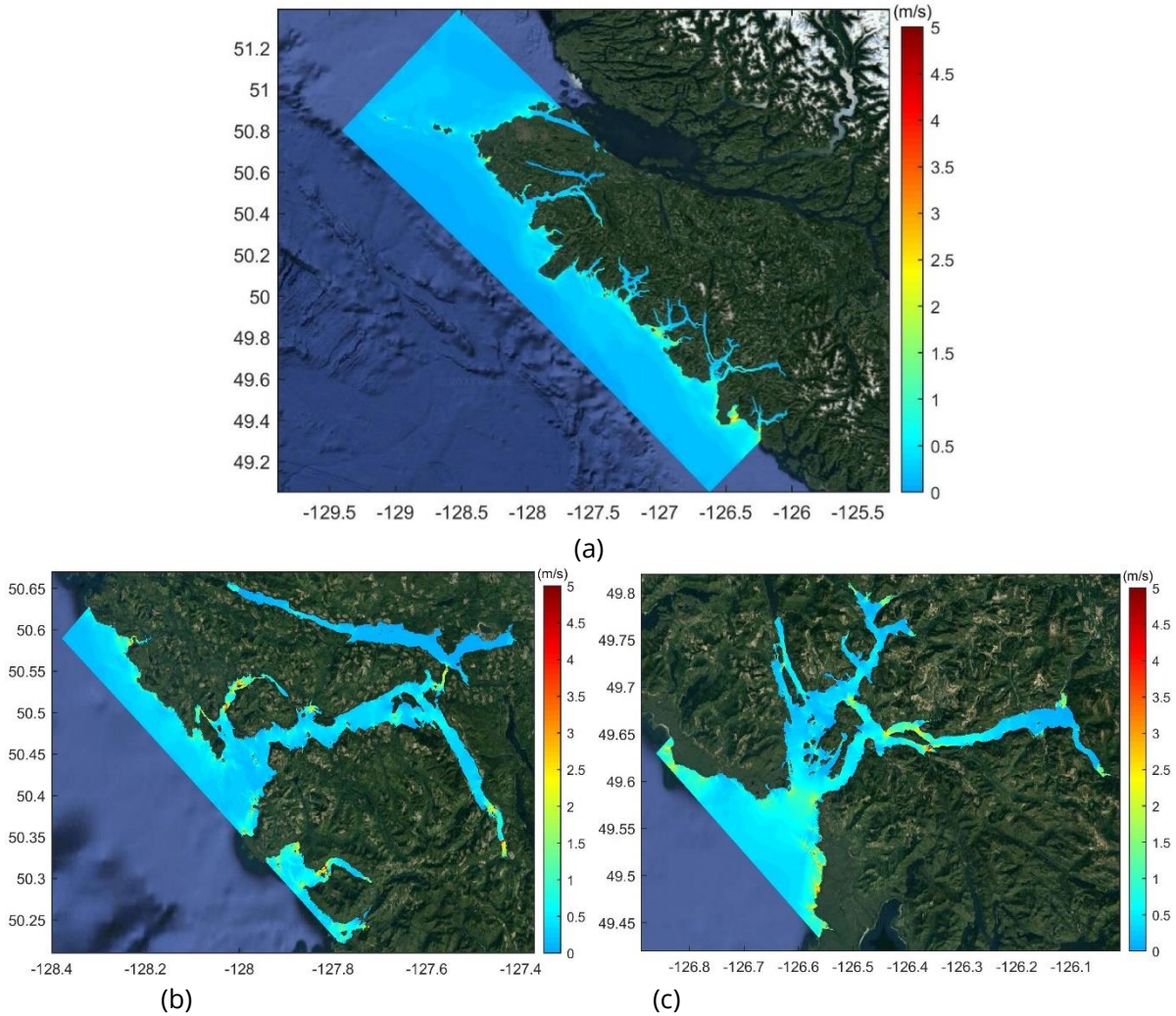

Figure C2: Maximum tsunami current velocities for Scenario4: Alaska-Aleutian Subduction Zone with 1.2m SLR a) 60 m resolution grid, b) 10m resolution grid of Quatsino, and c) 10m resolution grid of Nootka.

C.3 Time series of water surface elevation, of Nootka grid (0m, 1.2m SLR comparison)

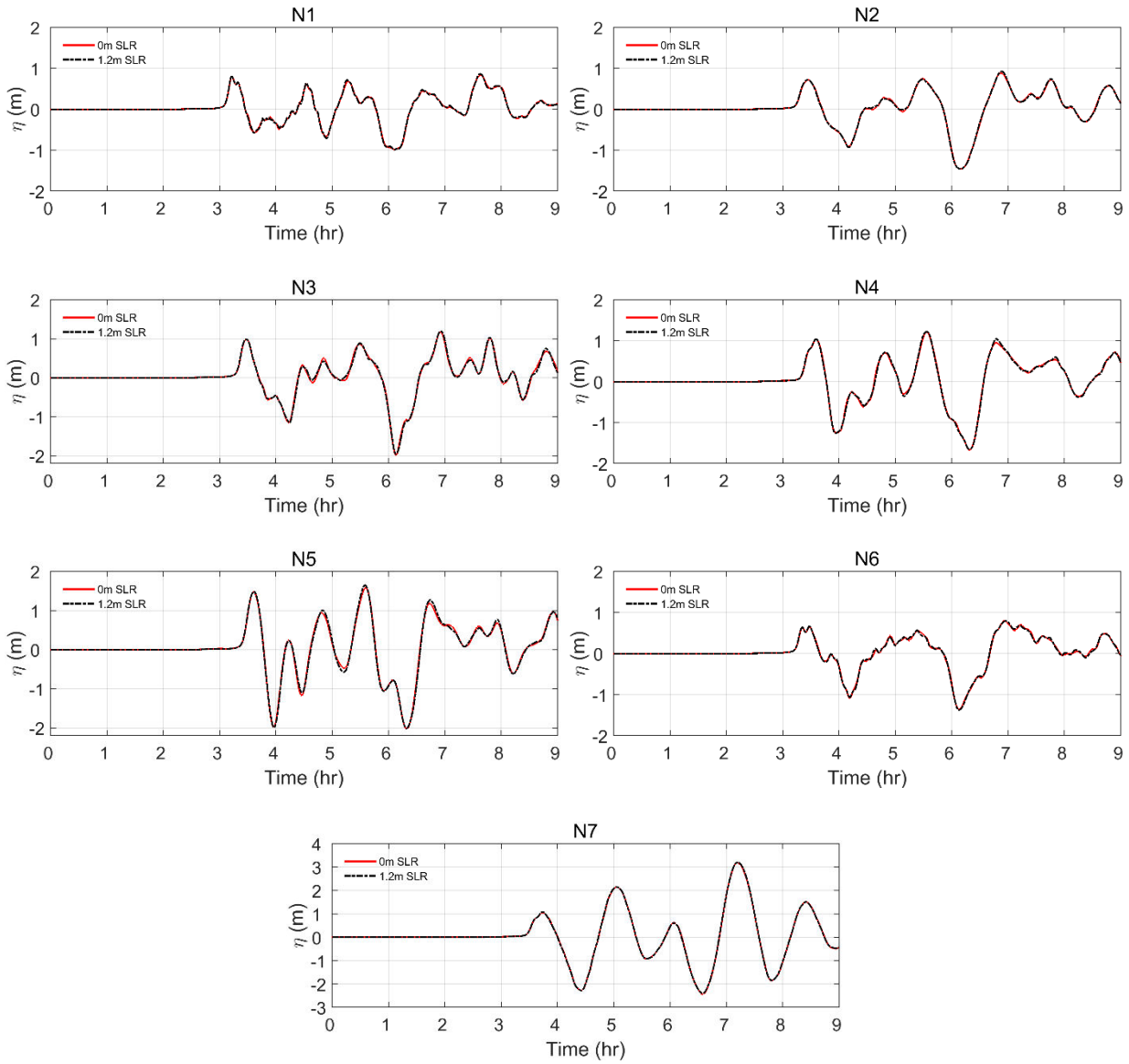

Figure C.3: Time series of water surface elevation for selected numerical gauge points of Nootka grid for present-day (0m SLR) and future scenario (1.2m SLR) from Alaska tsunami source. The water surface elevation (η) is with respect to HHWMT.

C.4 Time series of water surface elevation of Quatsino Sound (0m, 1.2m SLR comparison)

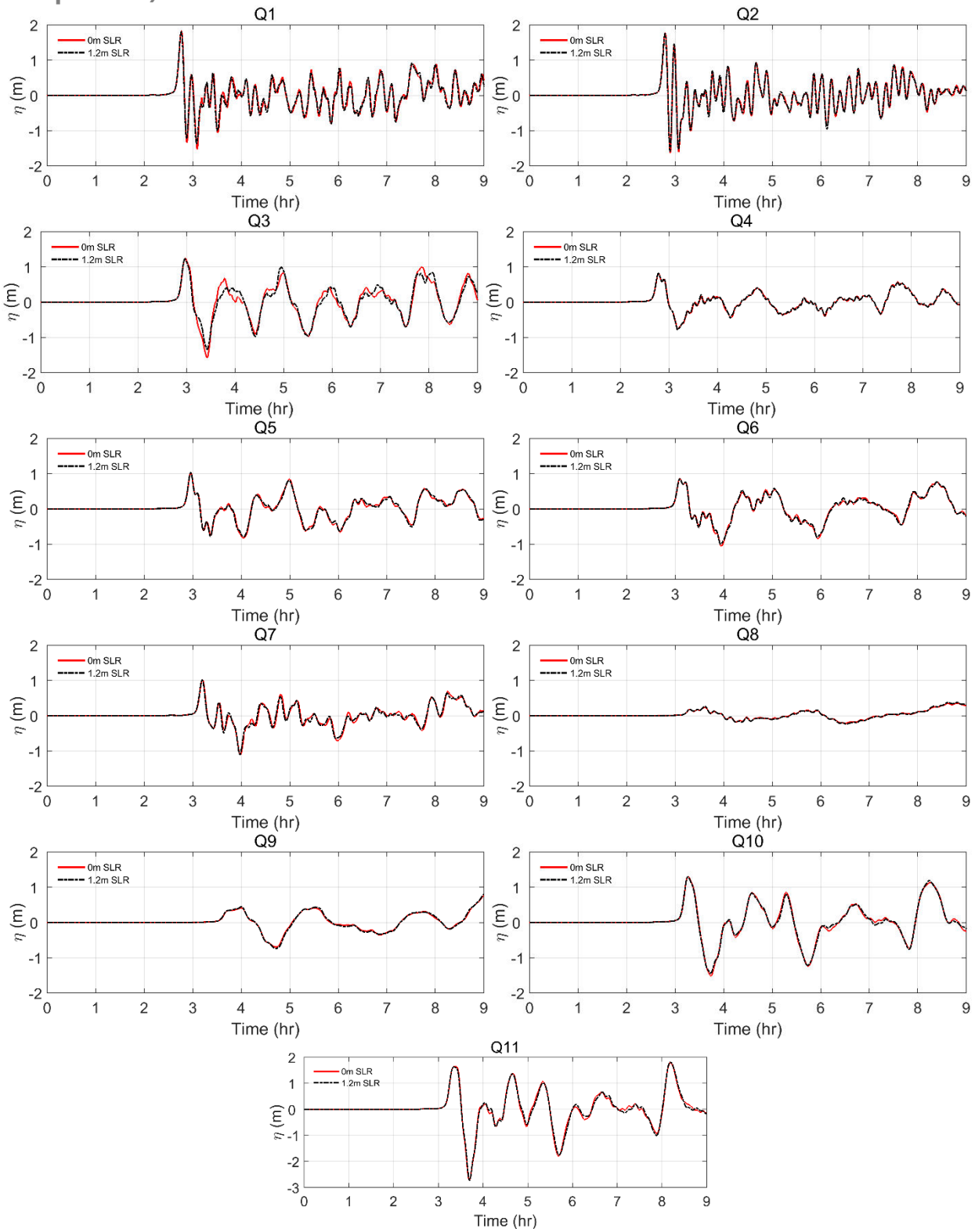

Figure C.4: Time series of water surface elevation for selected numerical gauge points of Quatsino grid for present-day (0m SLR) and future scenario (1.2m SLR) from Alaska tsunami source. The water surface elevation (η) is with respect to HHWMT.